January 2009

Reducing Energy Demand in Commercial Buildings: Balancing Convection and Radiant Cooling

Andrew Harris
Washington University in St. Louis

Recommended Citation

Harris, Andrew, "Reducing Energy Demand in Commercial Buildings: Balancing Convection and Radiant Cooling" (2009). *All Theses and Dissertations (ETDs)*. 440.
https://openscholarship.wustl.edu/etd/440

WASHINGTON UNIVERSITY IN ST. LOUIS

School of Engineering and Applied Science

Department of Mechanical, Aerospace, and Structural Engineering

Thesis Examination Committee:
Ramesh K. Agarwal, Chair
Kenneth L. Jerina
David A. Peters

REDUCING ENERGY DEMAND IN COMMERCIAL BUILDINGS:

BALANCING CONVECTION AND RADIANT COOLING

by

Andrew K. Harris

A thesis presented to the School of Engineering
of Washington University in partial fulfillment of the
requirements for the degree of

MASTER OF SCIENCE

August 2009
Saint Louis, Missouri

ABSTRACT OF THE THESIS

Reducing Energy Demand in Commercial Buildings:

Balancing Convection and Radiant Cooling

by

Andrew K. Harris

Master of Science in Mechanical Engineering

Washington University in St. Louis, 2009

Research Advisor: Professor Ramesh K. Agarwal

Using Computational Fluid Dynamics (CFD), three different cooling systems used in contemporary office environments are modeled to compare energy consumption and thermal comfort levels. Incorporating convection and radiation technologies, full-scale models of an office room compare arrangements for (a) an all-air overhead system (mixing ventilation), (b) an all-air raised floor system (displacement ventilation), and (c) a combined air and hydronic radiant system (displacement ventilation with a chilled ceiling). The computational domain for each model consists of one isothermal wall (simulating an exterior wall of the room) and adiabatic conditions for the remaining walls, floor, and ceiling (simulating interior walls of the room). Results show superior thermal comfort levels as well as substantial energy savings can be accrued using the displacement ventilation (b) and especially the displacement ventilation with a chilled ceiling (c) over the conventional mixing ventilation system (a).

Acknowledgements

Thanks to Professor Ramesh Agarwal for, not only his time and effort, but his resolve in advising me during this research. Also, thanks to Sesha Madireddi and Sai Putti Siu at Hussmann Corporation for helping me to understand the nuances of Fluent. Thanks to Lee Chusak for all of his consulting work while I learned the ropes of the CFD lab.

<div align="right">Andrew K. Harris</div>

Washington University in St. Louis
August 2009

Contents

List of Tables

List of Figures

x

Chapter 1

Introduction

1.1 Motivation

In recent years, greenhouse gas (GHG) emissions and their contribution to global climate change have been brought to the forefront of our everyday lives. Policymakers, commercial enterprises, and scientists are focusing attention on sources of energy and associated GHG emissions. There are two ways by which the GHG emissions can be lowered: (1) using clean sources of energy (non-fossil fuels) and (2) decreasing the energy consumption. Significant effort has been placed on renewable sources of clean energy such as Nuclear, Hydro, Clean Coal, Wind, Solar, Geothermal, Tidal Wave, etc. Unfortunately, due to cost, long lead times, proximity to populous zones, and other infrastructure problems, there is a dearth of near-term affordable solutions for clean energy. "Even in the most optimistic scenarios, most solutions require long lead times, on the order of decades, before they can make a substantial contribution to global energy supplies"[Glicksman, 2008].
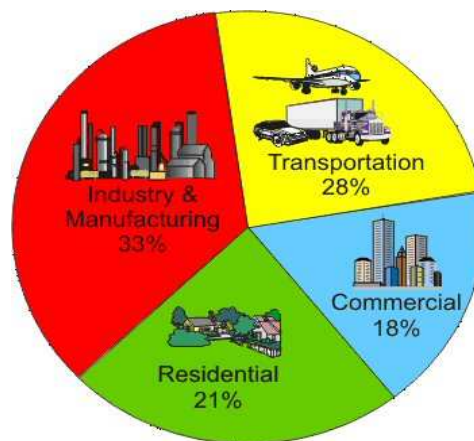
Figure 1.1 Energy Use in US by Sector [Carnegie Endowment for International Peace, 2009]

A more immediate rational approach to limiting global warming would be to place equal weight on curbing energy consumption through increasing efficiency until long-term, environmentally acceptable energy-supply technologies can be deployed at meaningful levels. The energy use chart (Figure 1.1) shows that the primary energy [1]use in the US can be categorized into four main sectors: industry, transportation, commercial buildings and residential buildings. Together the commercial and residential building sectors make up close to 40% of the total US primary energy usage, making them the largest sectors for energy consumption.

If we further group buildings from the other sectors to include structures from industrial, commercial, and transportation sectors, we can see from the charts shown in Figures 1.2 and 1.3, that buildings are responsible for almost half (48%) of all energy consumption and GHG emissions annually; globally this percentage is even greater. In terms of electricity consumption in the US, it can be seen from Figure 1.3 that 76% of all power-plant generated electricity is used for building operations.
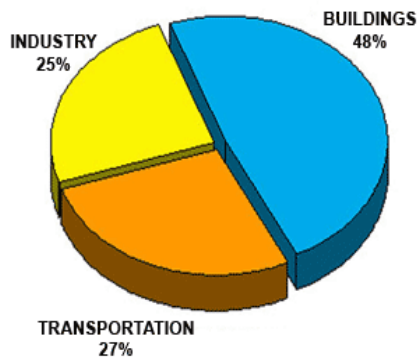
Figure 1.2 Energy use in US by sector [Architecture 2030, 2009]
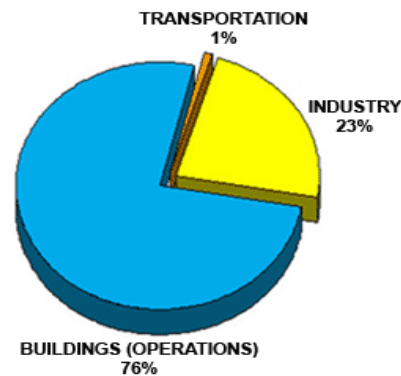
Figure 1.3 Electricity use in US by sector [Architecture 2030, 2009]

---

[1] Primary energy refers to the raw energy directly consumed, which includes the fossil energy and other energy sources needed to generate electricity. Electricity is not included as a separate end-use sector because it represents an intermediate conversion of energy rather than an end-use.

1.1.1   Overview of Energy Use in Buildings

When assessing the potential to reduce energy consumption in buildings, we must first breakdown the different uses of energy in order to see where the biggest gains in efficiency can be made. Moreover, the building energy usage depends upon different types of buildings constructed in various regional climates. Thus there won't be a one size fits all solution to making buildings more energy efficient. When examining the breakdown of energy use in the residential and commercial buildings in the US, European Union (EU), and Canada (Figures 1.4 and 1.5), we can clearly see that the single largest use of energy in these geographical regions is for space heating, followed by water heating. Similarly, space heating is the single largest use of energy in commercial buildings for the EU and Canada, accounting up to two-thirds of total energy use. Lighting can sometimes be the largest single use of electricity in commercial buildings, although in hot climates air-conditioning tends to be the single largest consumer of electricity.

1.1.2   Reducing Heating and Cooling

Heating and cooling loads are best reduced through the use of a high performance envelope (insulation, windows, air tightness) [Ürge-Vorsatz, Harvey, Mirasgedis, & Levine, 2007] combined with heat-recovery ventilation. Optimized building shape and orientation can also make a significant impact on heating and cooling loads, as can extensive equatorward-facing windows combined with internal thermal mass to avoid daytime overheating and to release stored heat at night. The European Passive House Standard and advanced houses in Canada and the US have achieved reductions in heating energy use by 75 – 90% in this way compared with the conventional practice [Ürge-Vorsatz, Harvey, Mirasgedis, & Levine, 2007].

1.2   Scope of the Thesis

1.2.1   2-D Model

Using Computational Fluid Dynamics (CFD) software, we will analyze 2-D and 3-D models of a single zone of the building (e.g. an office room). For the 2-D model, a closed domain with buoyancy driven flow is considered. The boundary conditions consist of two isothermal vertical walls (a hot and cold wall) and an adiabatic ceiling and floor allowing a direct comparison with the results of Olson, Glicksman, and Ferm, 2008.

1.2.2   3-D Models

For the 3-D models, different cooling techniques for modern office buildings are considered. All of the models consist of a computational domain representing a typical office room, with different ventilation systems providing the cooling. These 3-D models are used to compare three ventilation systems, (a) an all-air overhead system (mixing ventilation), (b) an all-air raised floor system (displacement ventilation), and (c) a combined air and hydronic radiant system (displacement ventilation with a chilled ceiling), for energy efficiency and thermal comfort levels. The full-scale models consist of one isothermal wall (simulating an exterior wall of the room) and adiabatic conditions for the remaining walls, floor, and ceiling (simulating interior walls of the room). Results show superior thermal comfort levels as well as substantial energy savings can be accrued using the displacement ventilation (b) and especially the displacement ventilation with a chilled ceiling (c) over the conventional mixing ventilation system (a).

U.S. Residential

- Miscellaneous 16%
- Furnace Fans 2%
- TVs 4%
- Clothes Dryers 3%
- Cooking 3%
- Lighting 6%
- Refridgerators 9%
- Water Heating 14%
- Space Cooling 8%
- Space Heating 35%

EU Residential

- Cooking 7%
- Lighting and Appliances 11%
- Water Heating 25%
- Space Heating 57%

Canada Residential

- Other Appliances 5%
- Lighting 5%
- Cooling 1%
- Major Appliances 8%
- Water Heating 21%
- Space Heating 60%
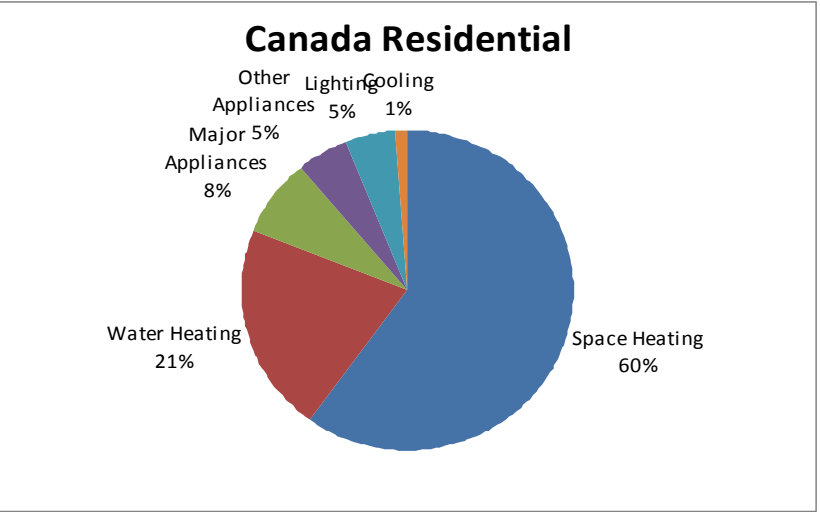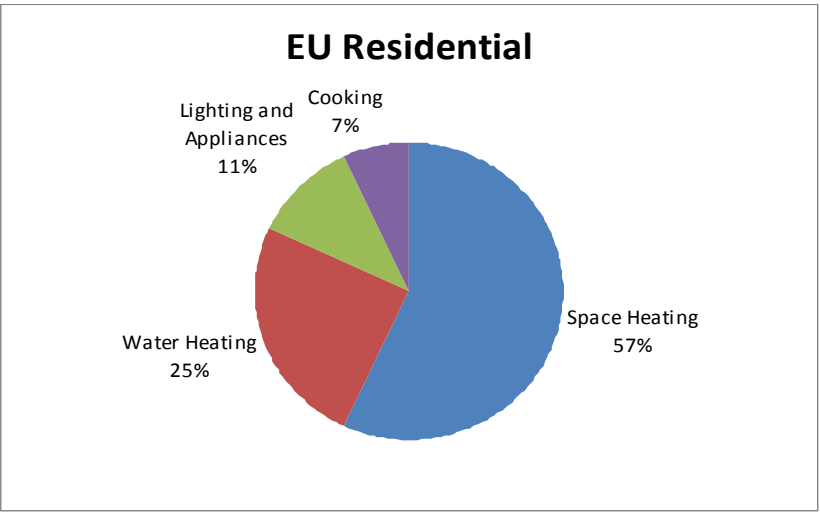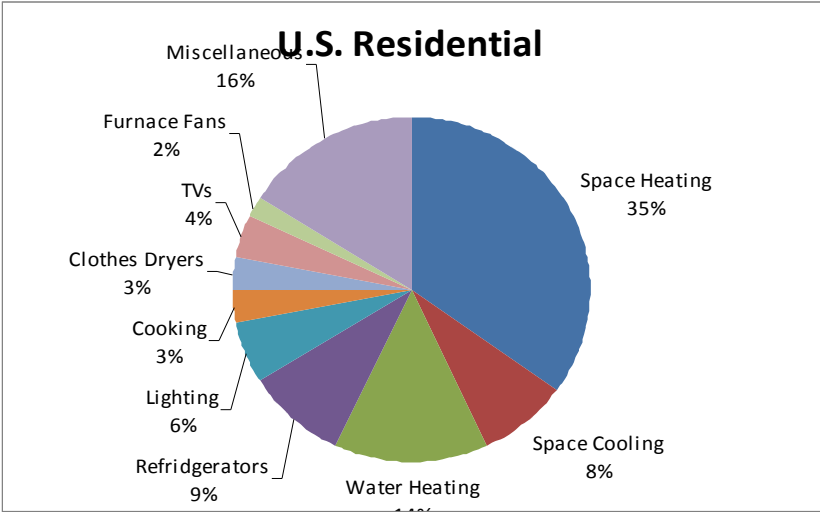
Figure 1.4 Residential energy use for the US [Koomey, 2000], EU [European Commission, 2001], and Canada [NRCan, 2005]

U.S. Commercial

Space Heating 13%
Space Cooling 7%
Water Heating 6%
Office Equipment 9%
Lighting 25%
Ventilation 4%
Refridgeration 4%
Miscellaneous 32%

EU Commercial

Other 16%
Cooling 4%
Cooking 5%
Lighting 14%
Water Heating 9%
Space Heating 52%

Canada Commercial

Lighting 13%
Auxiliary Equipment 20%
Water Heating 7%
Space Cooling 6%
Space Heating 54%
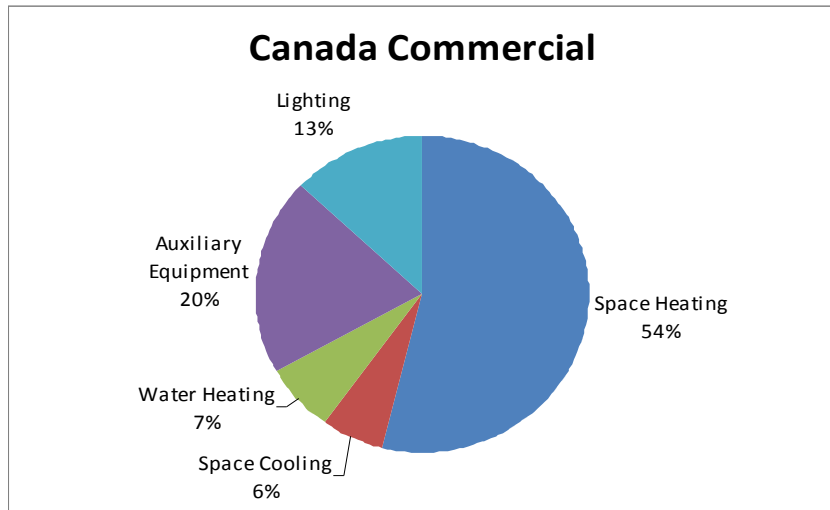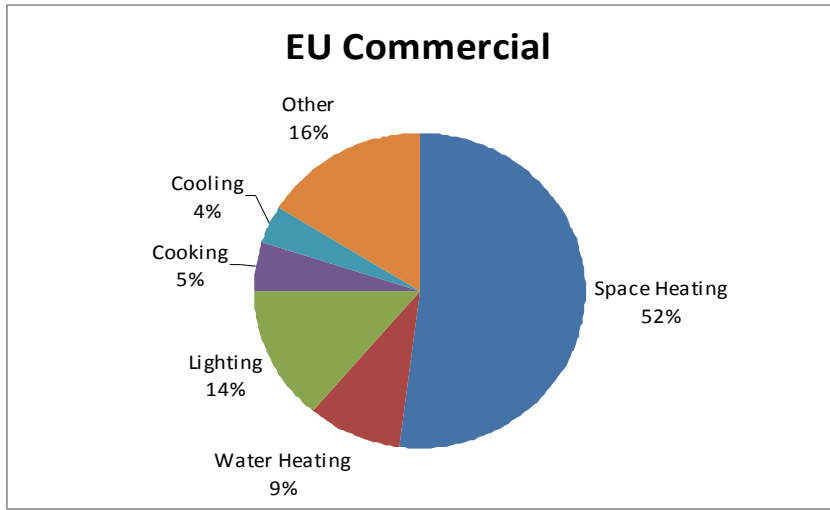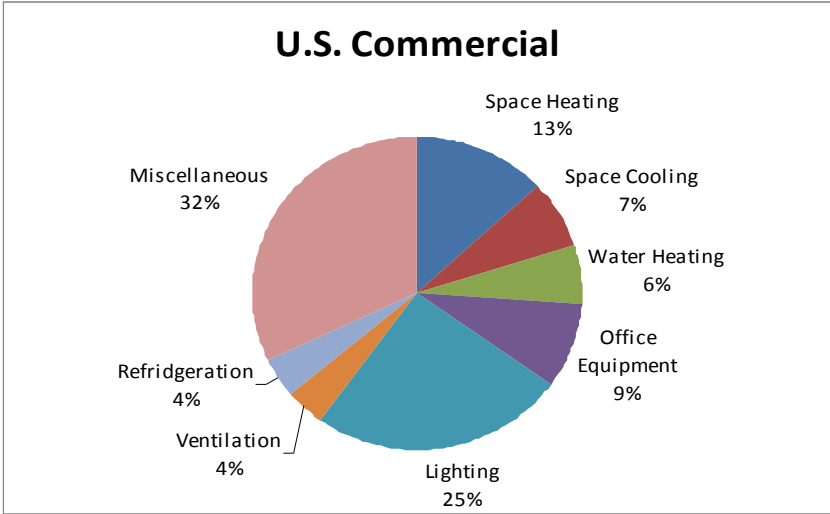
Figure1.5 Commercial energy use for the US [Energy Information Administration, 2009], EU [European Commission, 2001], and Canada [Natural Resources Canada, 2005]

Chapter 2

Ventilation Systems: Literature Survey

2.1 Conventional Variable-Air-Volume (VAV) Ventilation

In general, buildings, especially modern designs, are tightly constructed with low leakage rates from materials that provide high thermal insulation. In the simplest HVAC systems, where all-air overhead ventilation relies on turbulent mixing of room air with ventilated air, the mechanical air-conditioning must overcome the internal heat loads in a very direct way. The internal heat loads typically consist of heat plumes created from occupants, lights, and office equipment (including electronic devices on standby). The conventional office and industrial building design criteria for ventilation are based on the need to remove this excess heat (and pollutants) rather than to provide adequate air for respiration. A person requires about 7.5 liter/sec for respiration, while typical air changes needed for thermal comfort require at least ten times this amount [Linden, 1999].

In addition, for the typical mixing system, initial construction costs are low and it requires little maintenance; however, because of the large volume of air needed for heat exchange, this results in an increase in space allocation in comparison to the alternative systems. This increased space requirement typically results in greater building envelope surface area, and an associated increase in envelope heating and cooling loads. Given these factors, it is reasonable to assume that considerable inroads towards energy efficiency can be made by modifying these traditional HVAC systems.

2.2　Displacement Ventilation

A superior system is the displacement ventilation (DV) in which ventilated air is dispersed at low speeds along the floor (or near the floor along the walls) and is warmed by internal heat sources (occupants, lights, plug-in equipment) as it rises to the top, displacing the air already present. DV is more effective at removing contaminants than conventional turbulent mixing ventilation, while permitting a smaller airflow rate by a factor of two [Ürge-Vorsatz, Harvey, Mirasgedis, & Levine, 2007]. In addition, the supply air temperature for DV is significantly higher for the same comfort conditions (about 18° C versus about 13° C in a conventional mixing ventilation system), reducing the chilling load significantly. Depending on the regional climate, DV can reduce energy use for cooling and ventilation by 30-60% [Bourassa, 2002; Howe, 2003].

2.3　Displacement Ventilation with Radiant Cooling

The radiant (hydronic) heating/cooling system provides even greater potential for energy efficiency. Water is 25-100 times more effective than air at transferring heat energy. Thus, tremendous efficiency gains can be made by decoupling the ventilation from the heating/cooling load. In general, this decoupled system circulates chilled or hot water through the ceilings and walls of office buildings and the floors of residential units for temperature control, while only distributing the volume of air required for ventilation. This decoupled system allows for 100% of the ventilated air to be from the outside rather than re-circulating a portion of the indoor air, thereby providing health benefits. For example, it is not uncommon for conventional HVAC systems to recirculate up to 80% of the internal air on each circuit and replace the remaining 20% with fresh air [Harvey, 2009]. Also, further energy gains are achieved because the internal heat plumes generated by occupants, lighting, and plug-in equipment (constituting up to 30% of total cooling requirement [Harvey, 2009]) are vented directly outside rather than partly re-circulated, as in a conventional system. Using a decoupled system with constant ventilation can produce savings of 20-30%. It should be noted that the required airflow – now decoupled from heating/cooling functions – can be

made to vary with changing building occupancy. A demand controlled ventilation (DCV) system uses CO_2 and/or other sensors to adjust the ventilation rate, this can reduce total HVAC energy by an additional 20-30% when compared with a fixed rate ventilation based on maximum occupancy [Brandemuehl & Braun, 1999].

In a chilled ceiling system, a large fraction of the ceiling is chilled by circulating cool water through pipes or lightweight panels. In addition to the aforementioned increased effectiveness of water over air in transporting heat, there is a reduced cooling load since typically water is supplied at 16-20º C rather than 5-7º C, as in conventional hydronic cooling systems. Not only does this reduction in cooling load allows a higher chiller coefficient of performance (COP, or cooling power divided by fan power, a direct measure of efficiency), but it also allows more frequent use of 'water-side free cooling', where the mechanical chilling is bypassed altogether and supplied water for space cooling directly comes from cooling tower. As an example, if chilled water is supplied at 18° C, a cooling tower could provide the cooling requirements 97% of the time in Dublin, Ireland, and 67% percent of the time in Milan, Italy [Costellor & Finn, 2003].

In the case of conventional dehumidification systems with air-conditioning, dehumidification is accomplished by overcooling the air so that sufficient water vapor is condensed, and then the air is reheated to be supplied at a comfortable temperature. Dehumidification can be decoupled from cooling through a variety of desiccant-based techniques, with energy use savings of 25-30%, or by up to 50% if solar heat is used to regenerate the desiccant [Harvey, 2006].

Lastly, perceived temperature depends on more than just air temperature and its velocity. Infrared radiation from surrounding surfaces also plays a role, especially if there is significant radiant asymmetry. Infrared radiation depends on the temperature and emissivities of the surfaces enclosing the occupied space. As a result, radiant asymmetry happens when there is one surface, such as a window or exterior wall, is much hotter than other surfaces, such as the interior walls. Likewise, humans emit infrared radiation and if the emission of the surrounding surfaces and its subsequent absorption is greater than that of the human, then the person will feel warm even if the air is cool. Therefore, in the case of radiant cooling, the

set points for temperature and humidity can be adjusted higher due to the perceived temperature difference from traditional ventilation systems.

2.4   Market Failures

Implementation of new energy efficiency technologies and strategies face a plethora of obstacles to overcome. First, the building industry is very conservative and reluctant to accept technologies that are often incomplete, unavailable, expensive, and difficult to obtain or trust. Second, the industry is widely fragmented with a huge number of suppliers, builders, designers and developers, and lacks vertical or horizontal integration [Glicksman, 2008]. This fragmentation of the industry largely impacts the creation of a high performance envelope[2], which is the single most important factor in the design of low-energy buildings. Third, building manufacturers are divorced from operating costs. The standard within the industry is to construct a building with minimum up-front cost with little or no regard for the operating costs. Fourth, it is the practice in many countries to subsidize the primary energy and electricity, creating a disincentive for energy efficiency. Particularly, this is the case in many developing countries, and historically it has been the situation in Eastern Europe and the former Soviet Union. Fifth, non-payment and electricity theft has been occurring at a large scale in many countries. Developed countries are not immune to this practice; in US, this electricity theft and non-payment is estimated to cost utilities billions of dollars each year [Ürge-Vorsatz, Harvey, Mirasgedis, & Levine, 2007]. This practice encourages thieving parties to induce waste and discourage energy efficiency.

---

[2] Minimizing energy use requires optimizing the system as a whole by systematically addressing building form, orientation, envelope, glazing area, and host of interaction, and control issues involving the building's mechanical and electrical systems. This is more evident in larger, commercial buildings; but is present to some degree even in smaller residential and non-residential buildings. However, the division of responsibilities in the typical design process often contributes to suboptimal results.

Chapter 3

Computational Fluid Dynamics (CFD) Solver

Two ANSYS computer programs are used for the numerical simulations. GAMBIT [Ansys Inc, 2007] creates the office room geometry and generates the mesh inside the room while FLUENT [Ansys Inc, 2007] solves for the flow field and heat transfer.

3.1   GAMBIT

GAMBIT is a geometric modeling and grid generation software. It allows users to create or import geometry from most CAD packages. Meshing surfaces and volumes can be generated automatically while allowing the user to control the mesh spacing through the use of sizing functions and boundary layer meshing near the walls. There are many meshing options that allow the user to create a structured, unstructured, or a hybrid structured/unstructured mesh. In addition, there is a "body-fitting" mesh technology, which can easily mesh large, complex geometries or repair surface meshes.

After meshing the geometry, GAMBIT allows the user to group elements on which boundary conditions can be specified. These boundary conditions include the pressure outlet/inlet, velocity outlet/inlet, mass flow inlet/outlet, no-slip wall, and axis of symmetry conditions. Elements which are not part of the boundary conditions are assigned continuum parameters as either a fluid or a solid. Once the meshing process is completed, the file is exported to FLUENT, where all the elements and their designated conditions are integrated into a case file for processing.

11

3.2 FLUENT

FLUENT is a general-purpose CFD code, which solves the Unsteady Reynolds-averaged Navier-Stokes (URANS) equations using the finite-volume method on a collocated grid. It can model fluid flow and heat transfer in complex geometries using an interactive, menu-driven interface. It can solve 2- and 3-D problems in steady and unsteady simulations. FLUENT has the capability to solve incompressible and compressible flows using inviscid, laminar, and turbulent viscosity models. There is a wide array of turbulence models available, including Spalart-Allmaras (S-A), k-ω, and k-ε (standard, RNG, Realizable) models. Each turbulence model has its own separate options to change parameters for specific cases. When adapting an existing mesh for additional grid refinement, features are imported without changing the original mesh file from GAMBIT.

FLUENT provides output options for simulations involving fluid flow and heat transfer. Contour and live plots can be made for the desired variables/functions, including static temperature, total energy, entropy, etc. Furthermore, there are many post-processing options which make it easier to visualize and the calculated flow field data.

Chapter 4

2-D Model of Natural Convection in a Room

4.1   Introduction

The aim of this computation was to simulate a buoyancy-driven flow inside a 2-D rectangular enclosure for the purpose of validation. A 2-D closed rectangular domain with a length to height ratio of 3:1 was considered to compare the flow field results with those obtained experimentally by Olsen, Glicksman, and Ferm (1990). The flow in the enclosure is governed by the gravity driven natural convection current created by the hot and cold vertical walls with an adiabatic top and bottom horizontal walls (Figure 4.1 & 4.4). Although the geometric configuration is simple, this buoyancy driven flow is difficult to compute since the flow undergoes laminar to turbulent transition near the wall as shown in the experimental studies of Olsen, Glicksman, and Ferm (Figure 4.8). Furthermore, the natural convection flow is a low velocity (low momentum) flow which is sensitive to small perturbations making the steady state computation difficult. It has been found to be particularly difficult to produce a truly 2-D flow in the rectangular geometry [Tieszen, Ooi, Durbin, & Behnia, 1998].

爻彡 Turbulent flow
===== Laminar flow
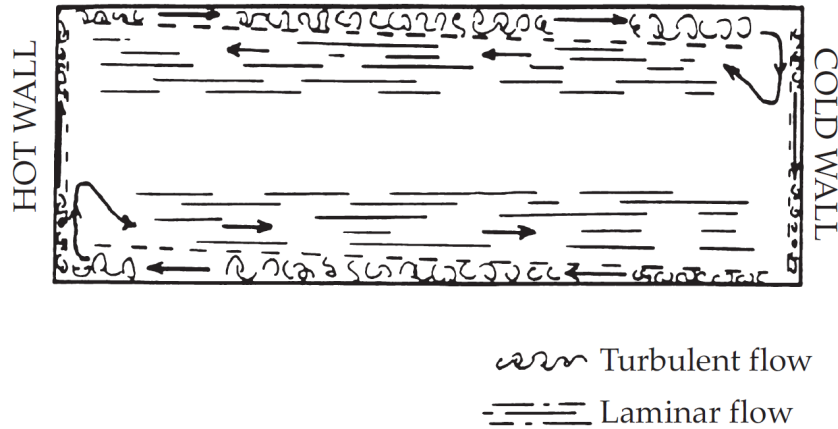
Figure 4.1 Experimentally observed flow pattern inside the rectangular enclosure [Olsen, Glicksman, & Ferm, 2008]

Figure 4.1 shows the sketch of the experimentally observed flow pattern in the rectangular box. The flow field shows the turbulent eddies near the wall, secondary recirculating flow in the corner regions, and laminar primary recirculating flow in the center region of the box away from the walls. The noteworthy aspect of this flow is that the turbulent flow near the walls circulates clockwise while the primary laminar flow in the center region circulates in the counterclockwise direction (Glicksman, 2008). Our goal in this chapter is to compute this flow field.

It is well known that near the wall of high Rayleigh number flows, there is an overlap of the viscous sub-layer and the fully turbulent outer layer (Figure 4.2) [Hölling & Herwig, 2006; George & Capp, 1979]. Since this wall region is important for heat transfer, it has been found that the wall treatment is very important in modeling buoyant flows [Ince & Launder, 1989; Henkes, 1990; Henkes & Hoogendoorn, 1989, 1995]. In previous work [Henkes, 1990], it has been found that for a hot plate at a Rayleigh number (Ra) $\approx 10^{11}$, the k-ε turbulence model without wall treatment resulted in a prediction of heat transfer 52% above the experimental values. With wall treatment, the resulting discrepancy between the computation and the experiment for heat transfer was reduced to $\pm 17\%$ [Henkes, 1990]. Figure 4.3 shows the typical temperature and velocity profile for natural convection from a vertical hot flat plate. Lastly, for an accurate numerical solution, the effects of thermal radiation should also be incorporated in the computations [Çengel & Turner, 2001; Howell & Potts, 2002].

14

It should be noted that there are important differences between the experimental setup of Olsen, Glicksman and Ferm (1990) and our 2-D computational model. In their experiment, a 3-D box was used with R114 gas as the testing fluid, whereas our computational model consists of a 2-D rectangular box with air as the test fluid. Furthermore, their experiments did not include the effects of radiation which is included in our computational model.
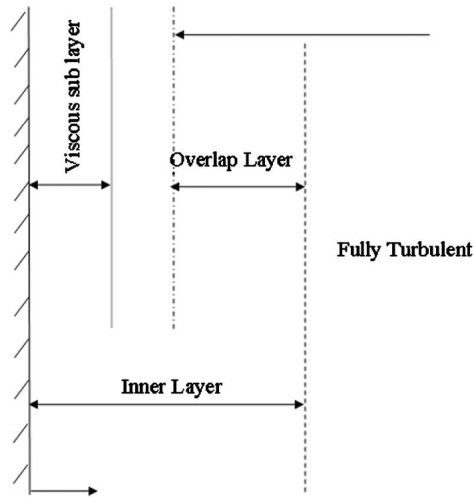
Schematic of two layer structure in the near wall region for high Rayleigh number flow due to natural convection from a vertical hot plate showing the viscous sub-layer, overlap, and the fully turbulent outer layer.

Figure 4.2 Boundary layer structure in natural convection on a vertical hot flat plate [Balaji, Hölling, & Herwig, 2007]
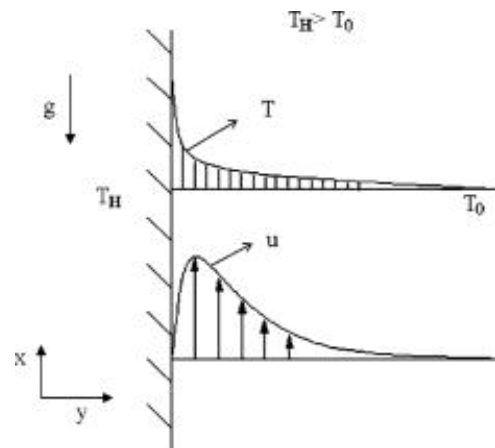
Turbulent natural convection from a hot vertical flat plate losing heat to quiescent air: velocity and temperature profiles at an axial location x.

Figure 4.3 Velocity and temperature profiles for natural convection from a vertical hot flat plate [Balaji, Hölling, & Herwig, 2007]

4.2   Mesh Generation

Gambit was employed for meshing the domain inside the rectangular box (Figure 4.4). A structured 100 x 100 Cartesian grid multiplied by a bi-exponent factor along both the vertical and horizontal directions was used to cluster the nodes near the boundaries (Figure 4.5). This was done to better resolve the steep flow gradients near the walls. For this mesh, the resulting node and cell counts are 10,201 and 10,000 respectively.

15
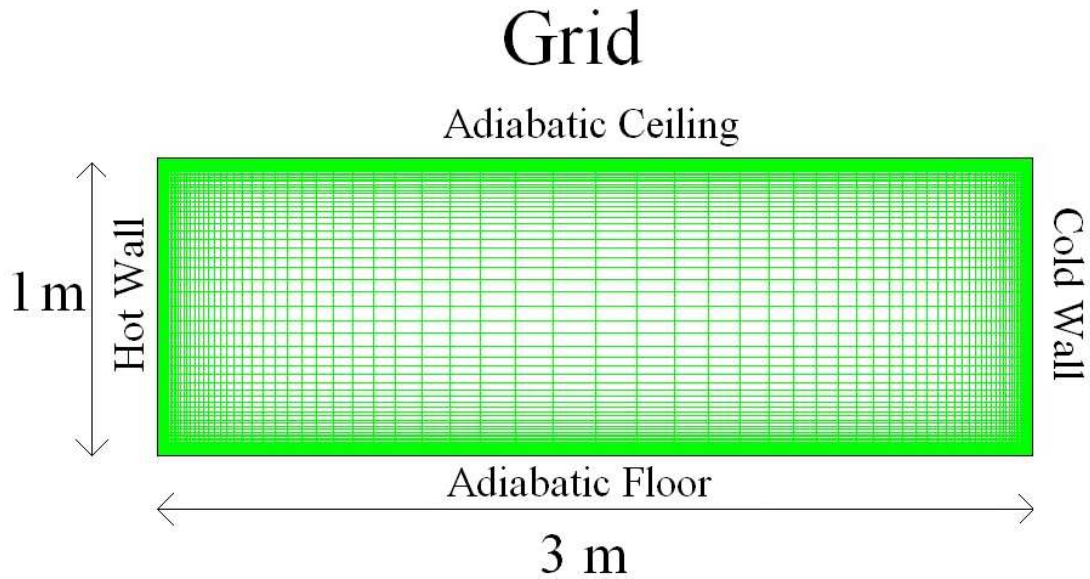
Figure 4.4 2-D mesh inside the rectangular enclosure

4.3 Flow and Heat Transfer Computations

4.3.1 Boundary Conditions

For the 2-D model of Figure 4.4 (3 meters x 1 meter), the following boundary conditions are imposed:

- Hot Wall: 305 K
- Cold Wall: 300 K
- Ceiling and Floor: adiabatic

4.3.2 Density Calculation

When considering buoyancy effect, because the expected temperature range for this study was slightly outside the applicable range of the Boussinesq approximation (<300 K) [Etheridge and Sandberg, 1996], the density of air was approximated as a function of temperature by a piece-wise linear approximation (Figure 4.5). The transient calculation was performed to achieve the steady state using the PISO algorithm in FLUENT to achieve the

16

coupling between the velocity and pressure. The first-order[3] upwind scheme was employed in the calculations with the exception of using the second order solver PRESTO! for pressure. The initial value for temperature, T_0=288.16 K, and the initial value for density, ρ_0= 1.225 kg/m^3, were specified.
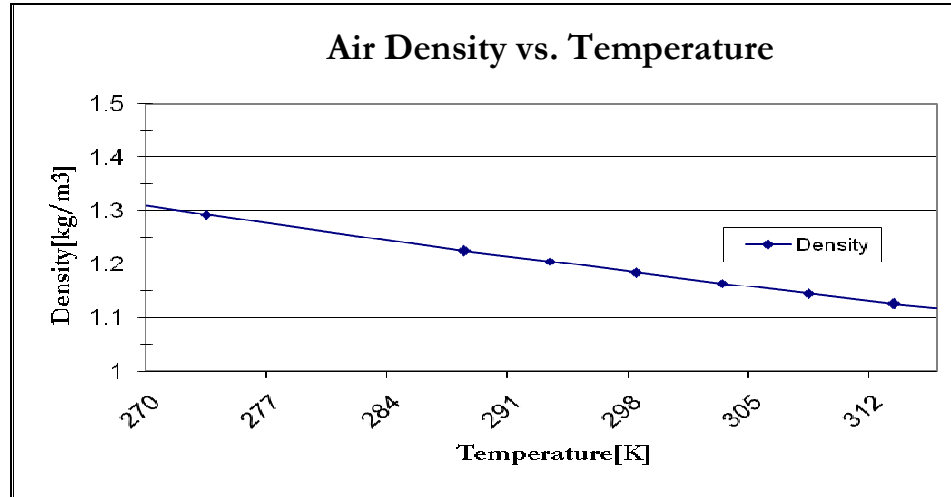
Figure 4.5 Air density vs. temperature [Appendix A]

4.3.3   Turbulence Model

Due to the presence of several flow regimes (laminar, transitional and turbulent) in buildings, there is not a single model of turbulence that can accurately describe the range of features generally found in room turbulence. The study of Howell & Potts (1998) has shown that the renormalization (RNG) k-ε turbulence model gives the best predictions of temperature stratification for a small room. Chen (1995) also suggested that the k-ε (RNG) turbulence model should be employed for simulating the building ventilation. Therefore, the k-ε (RNG) model with enhanced wall functions was employed.

4.3.4   Radiation Model

To account for the effects of radiation, the Discrete-Ordinates (DO) radiation model is employed [Ansys Inc, 2007]. The absorption coefficients for the wall material is assumed to be 0.85 and for the water vapor in air, it is taken to be 0.17 [ASHRAE, 1977].

---

[3] Note: the differences between the results using the first and second-order upwind schemes were negligible.

4.4   Heat Transfer Calculations

The energy equation is used in FLUENT for heat transfer calculations.

4.4.1   Energy Equation

In FLUENT the following form of the energy equation is used:

$$\frac{\partial}{\partial t}(\rho E) + \nabla \vec{v}(\rho E + p) = \nabla\left(k_{eff}\nabla T - \sum_j h_j \vec{J}_j + \overline{\overline{\tau}}_{eff}\ \vec{v}\right) + S_h \tag{4.1}$$

In equation (4.1), k_{eff} is the effective thermal conductivity ($=k + k_t$, where k is the thermal conductivity of the fluid and k_t is the turbulent thermal conductivity defined in the turbulence model being used) and $\vec{J}_j$ is the diffusion flux of species j. The first three terms on right-hand side of equation (4.1) represent energy transfer due to conduction, species diffusion, and viscous dissipation respectively. S_h includes the heat of chemical reaction and other volumetric heat sources.

The total energy, E, is expressed in terms of static enthalpy:

$$E = h - \frac{p}{\rho} + \frac{v^2}{2} \tag{4.2}$$

Where h is enthalpy defined as $h = \sum_j Y_j h_j$ for an ideal gas; Y_j is mass fraction of species j.

From equations (4.1) and (4.2), the static temperature, T, can be calculated.

4.4.2   Heat Transfer at the Wall Boundaries

For a fixed temperature condition at the wall, the heat flux to the wall from the adjacent fluid is given by:

$$q = h_f \left(T_w - T_f \right) + q_{rad} \qquad\qquad (4.3)$$

where h_f is the fluid-side local heat transfer coefficient[4], T_w is the wall surface temperature, T_f is the local fluid temperature, and q_{rad} is the radiative heat transfer.

4.4.3 Heat Flux Boundary Conditions

When a heat flux boundary condition is defined at a wall, the surface temperature adjacent to a fluid cell is calculated by the equation (4.3) as:

$$T_w = \frac{q - q_{rad}}{h_f} + T_f \qquad\qquad (4.4)$$

where all the terms are the same as defined in section 4.5.2.

4.5 Results and Discussion

In this section, the results of computations for buoyancy-driven flow inside the rectangular box of Figure 4.4 are presented.

4.5.1 Flow Patterns

Figure 4.6 shows the computed contours of velocity magnitude and Figures 4.7 and 4.8 show the velocity vectors inside the box. Figures 4.9 and 4.10 show the zoomed-in view of the flow patterns in the left and right portions of the box respectively. These flow patterns

---

[4] The fluid-side heat transfer coefficient is computed based on the local flow field conditions

are qualitatively similar to the flow patterns observed in the experiments of Olsen, Glicksman, and Ferm (1990). Figure 4.11 shows the static temperature contours inside the box.

4.5.2   Boundary Layer

Figures 4.12 and 4.13 show the zoomed-in view of the velocity profiles on the vertical hot wall at y-50 location and the horizontal bottom wall at x-50 location respectively. It is interesting to note the difference in the velocity profiles in Figures 4.12 and 4.13. In Figure 4.12, the velocity first increases rapidly and then decreases after attaining a peak value. In Figure 4.13, the velocity profile shows a monotonic behavior.

The vertical boundary layer thickness in Figure 4.12, is between 1.75 to 5% of the enclosure height, which is similar to the 2-5% obtained in the experiment by Olsen, Glicksmam, and Ferm (1990). This variation in boundary layer thickness is due to the difference in the wall temperatures[5] in the computation and the experiment. The maximum computed vertical velocity in the boundary layer is 15 cm/s (Figure 4.12), which is close to that in the experiment of Olsen, Glicksman, and Ferm (1990). Inside the 2-D enclosure, the eddy formations are illustrated in Figures 4.8 - 4.10.

4.5.3   Secondary Flows in the Corner Regions

Figures 4.9 and 4.10 show the recirculating vortices in the corner regions of the box. Reasons for the formation of the secondary flow vortices in the corner regions are as follows. Near the ceiling, close to the hot wall, the momentum-driven horizontal wall-jet entrains fluid until it reaches near the cold wall. By this time, the mass flow is too great to be entirely entrained into the cold wall boundary layer. As the flow turns downward along the cold vertical wall, there is little heat transfer to the outer portion of the wall-jet. Since this

---

[5] In the experiment, for the full scale room, the temperature difference (ΔT) between the hot and cold wall was 12º - 20º C and for the 1:5.5 scale model ΔT was 30º C. In our model ΔT was 5º C. Olsen et al (1990) used a higher ΔT to achieve higher Rayleigh number (Ra).

outer portion of the wall-jet is still relatively warm compared to the core flow in the box, it loses momentum due to the upward buoyant force as it travels downward. Eventually, this upward buoyant force generates enough momentum to redirect the flow upwards generating secondary flow vortices. The outer flow turns back towards the hot wall and serves as a source of entrainment for the hot wall boundary layer [Olsen, Glicksman, & Ferm, 1990].

In figures 4.14 and 4.15, the velocity magnitude profiles along the x-50 and y-50 lines respectively, show steep velocity gradients along the walls, especially along the hot and cold vertical walls. In figures 4.16 and 4.17, the v-velocity profiles along the x-50 and y-50 lines respectively, show only the flow near the hot and cold vertical walls has substantial vertical movement. In figures 4.18 and 4.19, the u-velocity profiles along the x-50 and y-50 lines respectively, show significant horizontal movement in the center of the room, mainly near the adiabatic top and bottom walls, with little horizontal movement near the hot and cold vertical walls. In figures 4.20 and 4.21, the temperature profiles along x-50 and y-50 lines respectively, show steep temperature gradients near the hot and cold vertical walls.

In figures 4.22 and 4.23 show the comparison between the computed and experimental temperature profiles near the boundary of the hot wall. Figures 4.24 and 4.25 show the comparison between the computed and experimental temperature profiles along the vertical axis at the center of the box. Reasonable agreement between the computed and experimental profiles can be observed.
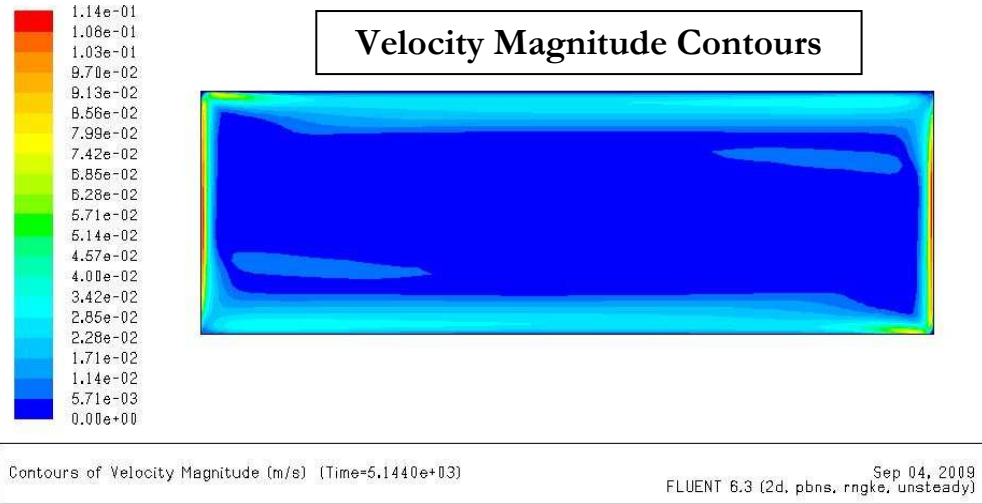
Figure 4.6 Velocity magnitude contours inside the rectangular enclosure due to buoyancy-driven flow
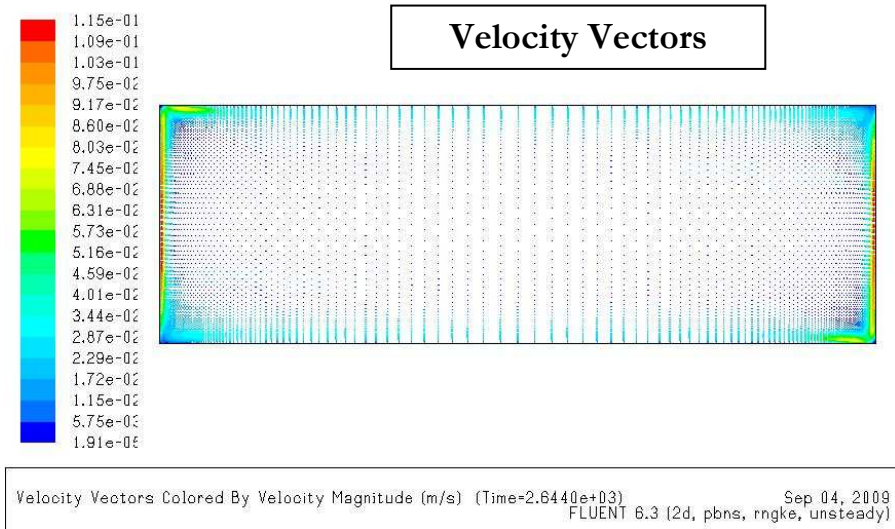

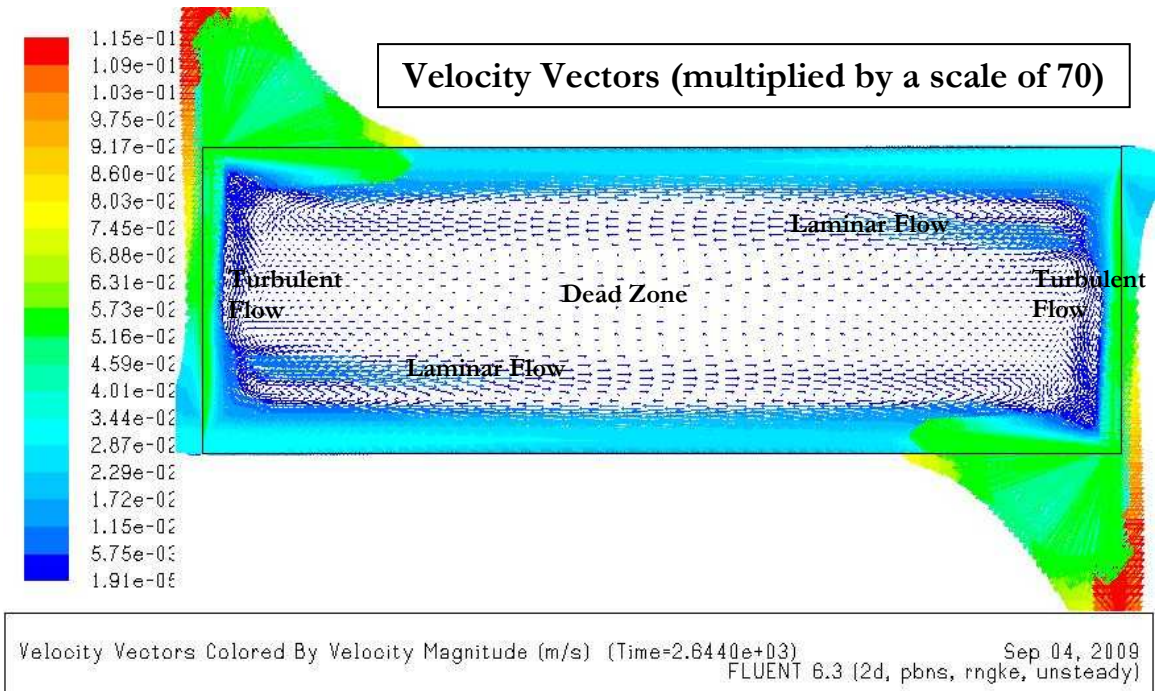**Figure 4.7 Velocity vectors inside the rectangular enclosure due to buoyancy-driven flow**

Figure 4.8 Velocity vectors (multiplied by scale of 70) inside the rectangular enclosure
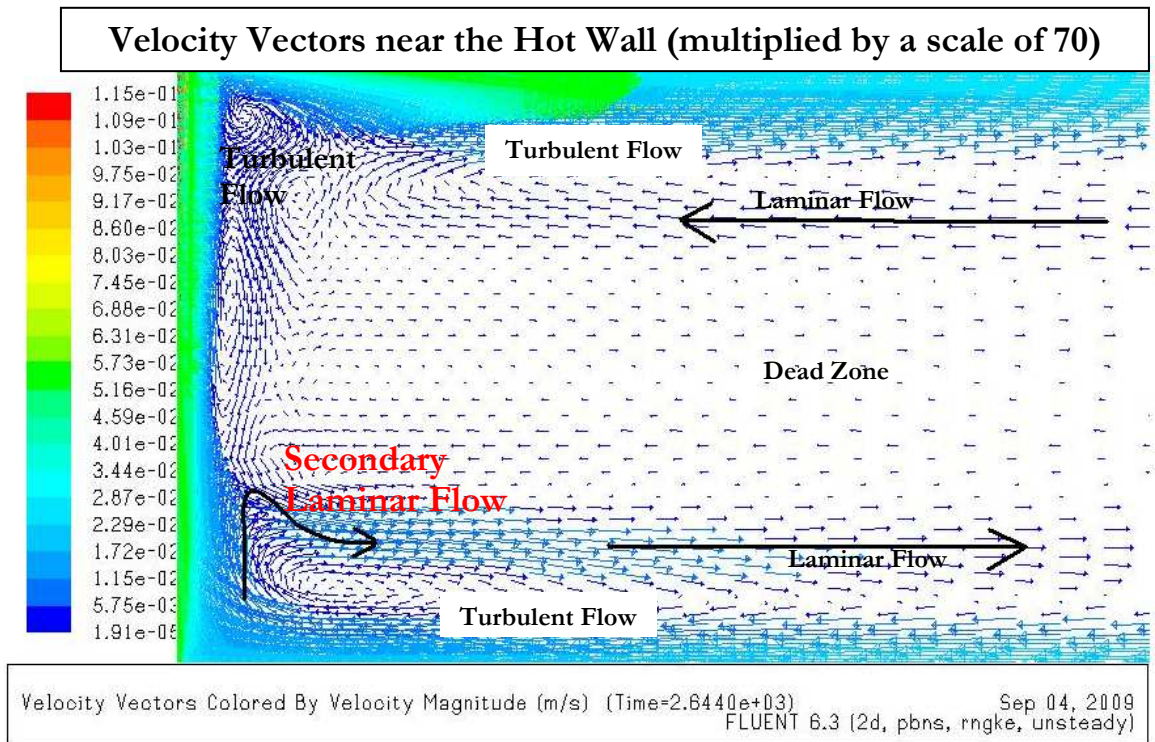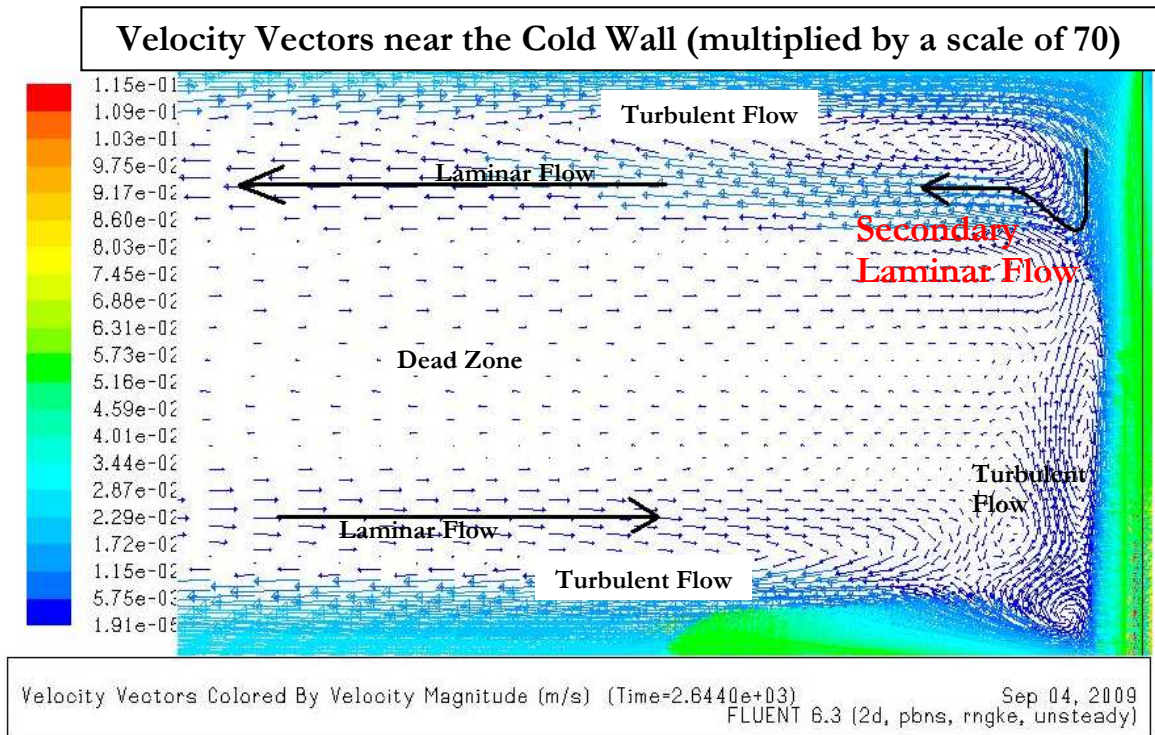

Figure 4.9 Velocity vectors near the hot wall region

Velocity Vectors near the Cold Wall (multiplied by a scale of 70)

1.15e-01	
1.09e-01	Turbulent Flow
1.03e-01	
9.75e-02	Laminar Flow
9.17e-02	
8.60e-02	Secondary
8.03e-02	Laminar Flow
7.45e-02	
6.88e-02	
6.31e-02	
5.73e-02	Dead Zone
5.16e-02	
4.59e-02	
4.01e-02	
3.44e-02	Turbulent
2.87e-02	Flow
2.29e-02	Laminar Flow
1.72e-02	
1.15e-02	Turbulent Flow
5.75e-03	
1.91e-05	

Velocity Vectors Colored By Velocity Magnitude (m/s) (Time=2.6440e+03)   Sep 04, 2009
FLUENT 6.3 (2d, pbns, rngke, unsteady)

Figure 4.10 Velocity vectors near the cold wall region

Temperature Contours

3.05e+02	
3.05e+02	
3.05e+02	
3.04e+02	
3.04e+02	
3.04e+02	
3.04e+02	Cold Wall
3.03e+02	
3.03e+02	Hot Wall
3.03e+02	Y-50
3.03e+02	
3.02e+02	
3.02e+02	
3.02e+02	
3.02e+02	
3.01e+02	
3.01e+02	X-25 X-50 X-75
3.01e+02	
3.00e+02	
3.00e+02	

Contours of Static Temperature (k) (Time=5.1440e+03)   Sep 04, 2009
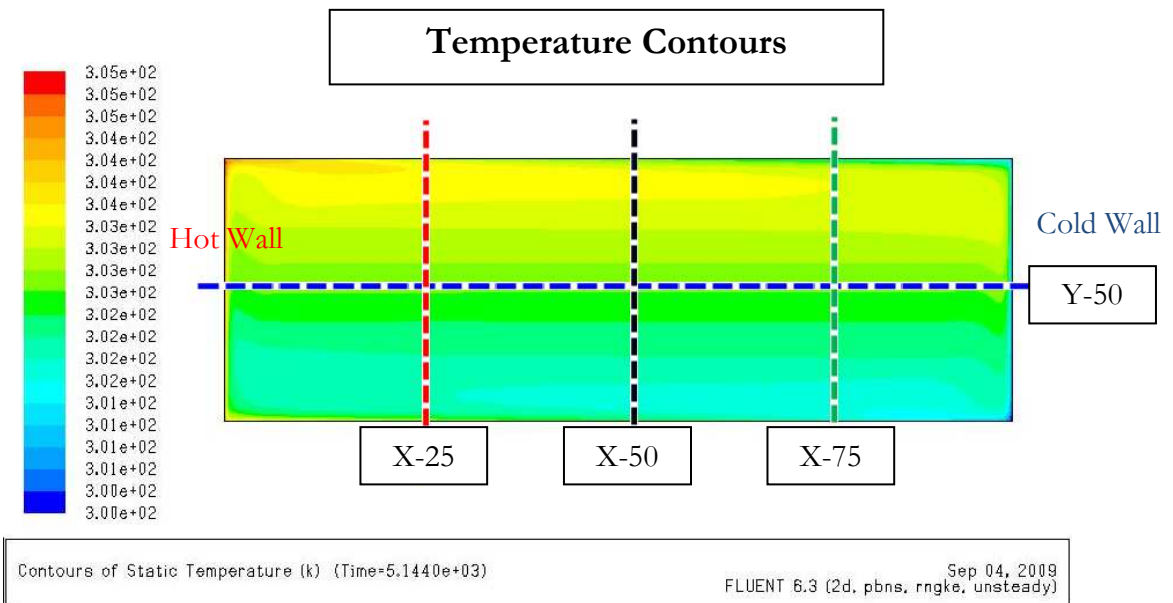FLUENT 6.3 (2d, pbns, rngke, unsteady)

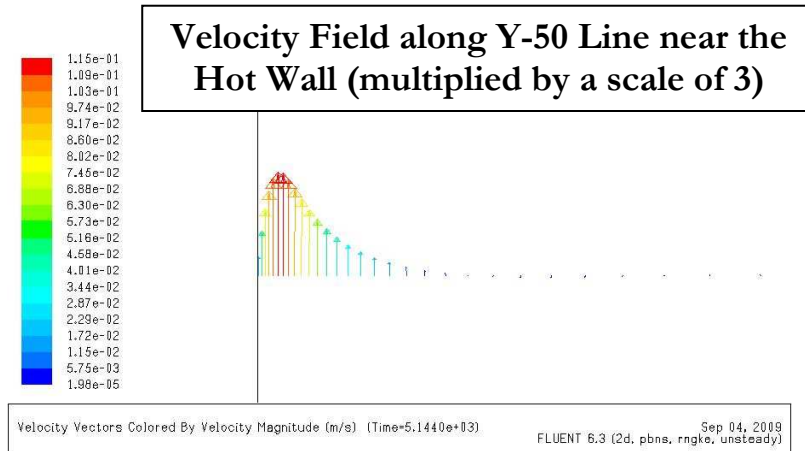**Figure 4.11 Temperature contours at x-25, x-50, x-75, & y-50**

Figure 4.12 Velocity field along the x-axis at y=50 near the hot wall boundary

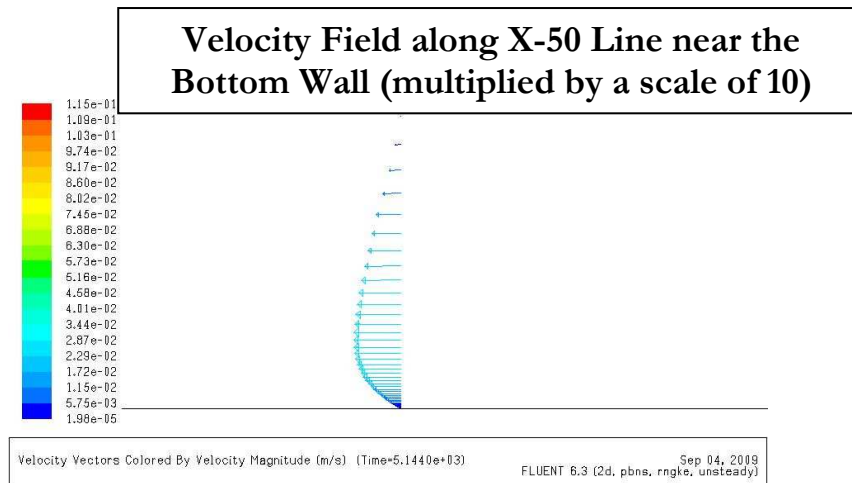Figure 4.13 Velocity field along the y-axis at x=50 near the bottom wall boundary
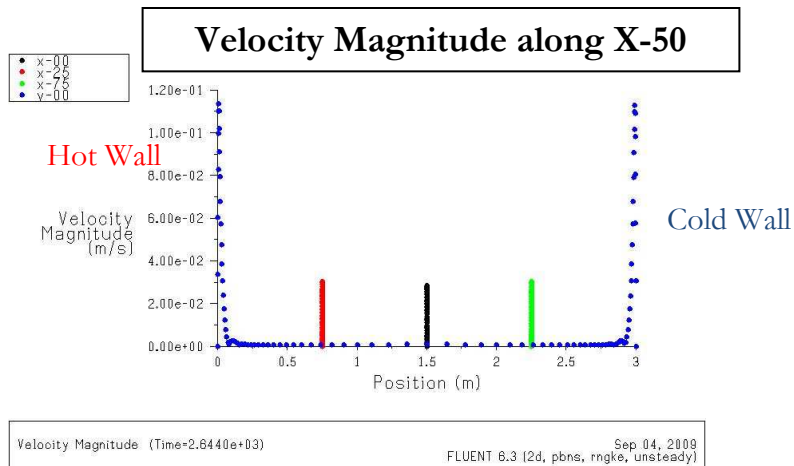

Figure 4.14 Velocity magnitude along x-50 line
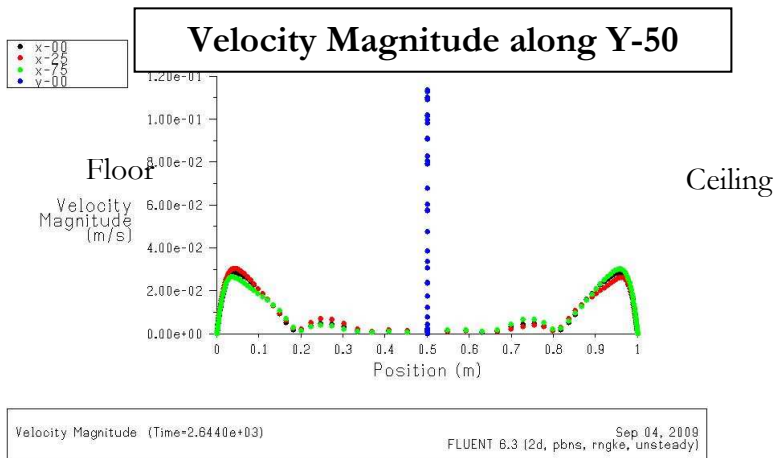
Figure 4.15 Velocity magnitude along y-50 line
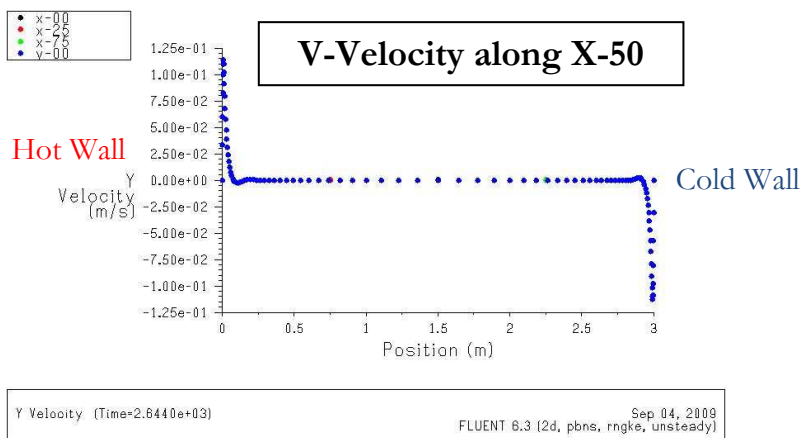

Figure 4.16 V-velocity along x-50 line
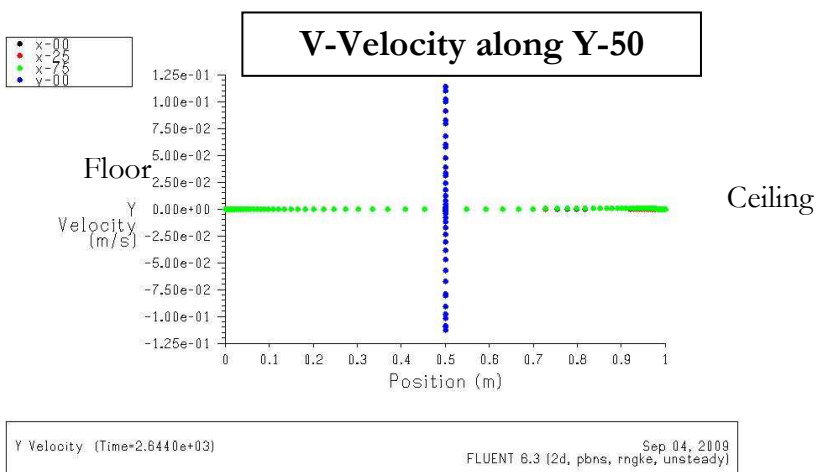
Figure 4.17 V-velocity along y-50 line

Figure 4.18 U-velocity along x-50 line

Figure 4.19 U-velocity along y-50 line

Figure 4.20 Temperature along x-50 line

27
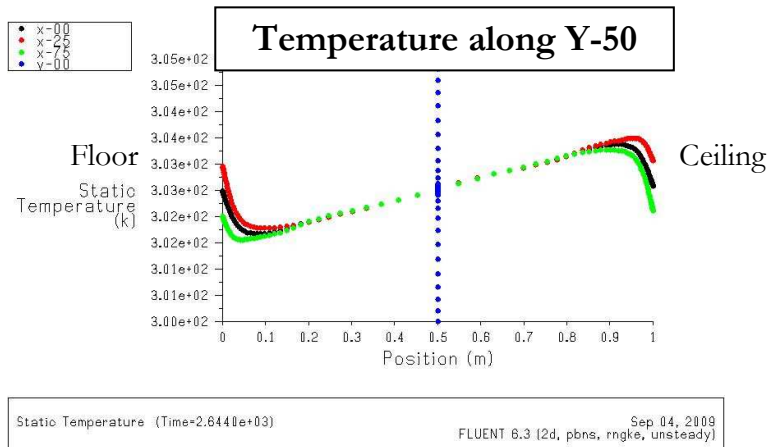
Figure 4.21 Temperature along y-50 line

Dimensionless Temperature Profile Near Boundary of Hot Wall
Comparison of Computed and Experimental Results
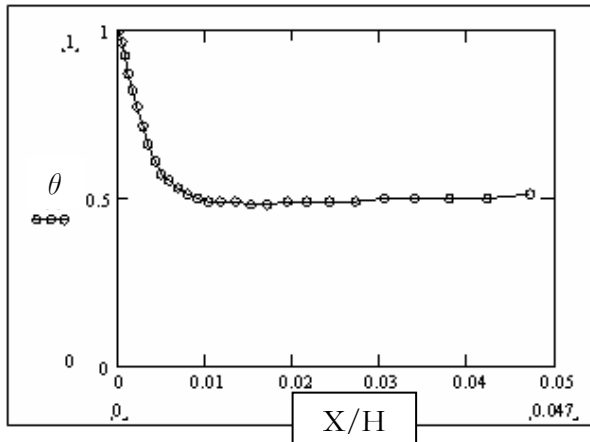
2-D model: Ra=2.6 x 10^8; ΔT=5 K

Figure 4.22 Computed dimensionless temperature at y-50
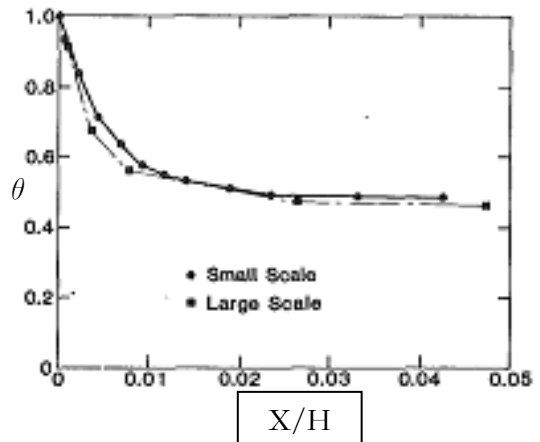
Comparison of small-scale and full-scale hot wall boundary layer temperatures along center of the room (at Z/H = 0.5). Small scale: Ra=3.1 x 10^{10}, ΔT=18.4 K; full scale: Ra=3.4 x 10^{10}, ΔT=30.0 K

Figure 4.23 Experimental dimensionless temperature profile of observed flow [Olsen, Glicksman, & Ferm, 1990]

Dimensionless Temperature Profile Along Vertical Axis
Comparison at the Center of the Enclosure
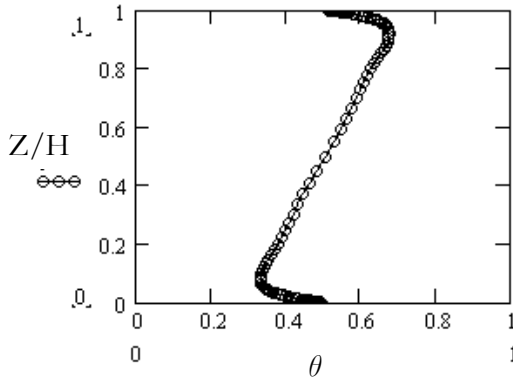
2-D model: Ra=2.6 x 10^8; ΔT=5 K

4.24 Computed dimensionless temperature profile at x-50
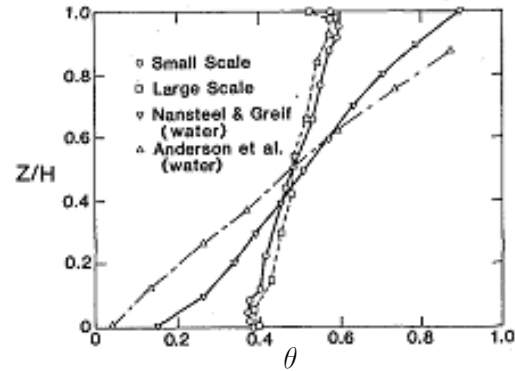
Comparison of core vertical temperature profiles at X/L = 0.5 in the empty enclosure for small-scale, full-scale, and water experiments. Small scale: Ra=2.2 x 10^10, ΔT=20.5 K; full scale: Ra=2.6 x 10^10, ΔT=15.4 K.

4.25 Experimental dimensionless temperature profile [Olsen, Glicksman & Ferm, 1990]

4.6   Conclusions

In this chapter, we have attempted to show that the 2-D flow field of natural convection in a rectangular box can be accurately calculated using CFD. The computations compare remarkably well with the experiment of Olsen, Glicksman and Ferm (1990) for flow patterns inside the box capturing the turbulent, laminar, and secondary laminar recirculating regions inside the box. Minor differences are found between the computation and experiment for the temperature profiles; it is likely that these small differences in the thermal stratification may be due to the different fluids used in the experiment (R114 gas) and the computation (air), since the air will have slightly more thermal stratification than the R114 gas.

There are other differences between the computation and the experiment as well; the computation is strictly 2-D while the experiments are performed in a 3-D enclosure. Nevertheless, there is reasonable agreement between the computation and the experiment. CFD validation in this chapter sets the stage for 3-D computations described in Chapter 5 of buoyancy-driven flow field in an office room using the three ventilation systems described in Chapter 2.

Chapter 5

3-D Models of Different Ventilation Systems

5.1   Introduction

The goal of the computations performed in this chapter is to directly compare the energy consumption and thermal comfort levels of three different ventilation systems described earlier in Chapter 2. For the computational domain, a typical office room space of approximately 12'-0" x 12'-0" x 9'-6" inside a multi-floor building is considered. In Figure 5.1, the first model (Room 1) uses an all-air overhead arrangement or variable air volume (VAV) system (Figure 5.1 (A)), representative of a conventional ventilation system. The second model (Room 2) uses an all-air raised floor arrangement, representative of the Displacement Ventilation (DV) system (Figure 5.1 (B)). The third model (Room 3) uses the combined DV and hydronic radiant systems (Figure 5.1 (C)).

(A) Variable Air
 Volume Ventilation
System

(B) Under-floor Dis-
placement Ventilation
System

(C) Combined Dis-
placement Ventilation
and Radiation System

Figure 5.1 Ventilation systems for an office building

Fresh Air Supply
Return Air
Radiant Chilled Ceiling
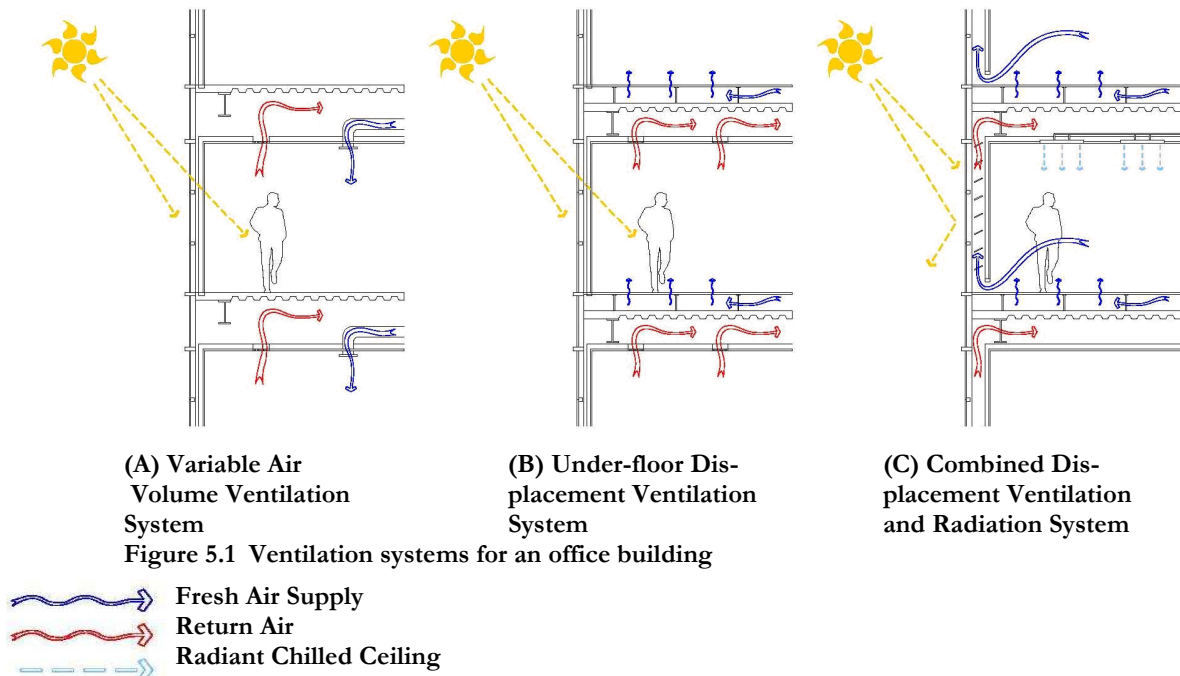
5.2   Computational Methodology

Figure 5.2 Temperature variation during a cooling cycle

Computational simulations are performed for the three ventilation systems shown in Figure 5.1 along the exterior wall of a model 3-D room of 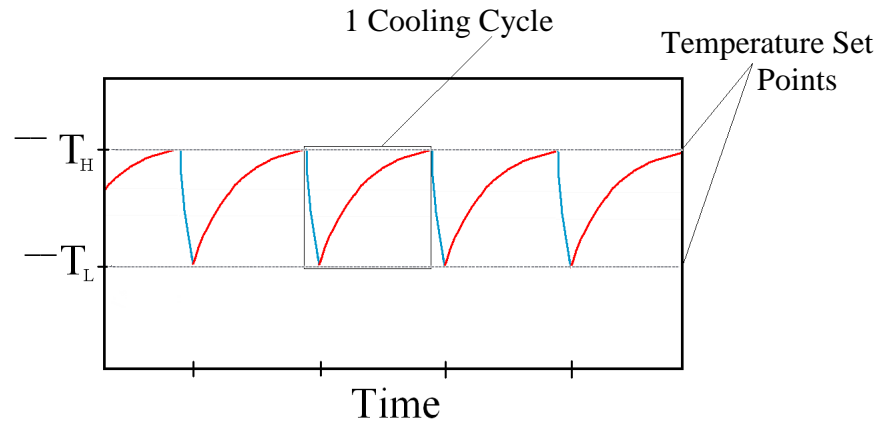12' x 12' x 9.5' dimensions. The cooling cycle shown Figure 5.2 is employed in the simulation; it shows the typical temperature curve during the hot part of the day. The red curve indicates the rising indoor temperature, caused by the hot interior and exterior sources, while the blue curve indicates the decrease in the indoor temperature due to the cold air supplied by the vents. Figure 5.2 also indicates the high and low temperature points inside the room, which are set by the controller (governed by the room occupant). Since we have not coupled our fluid dynamic simulations with the controller, we simulate the effect of the controller by opening the vents for ten minutes with the required amount of cold air as given in Table 5.1 and then closing the vents for remainder of the ninety minute cycle. This is obviously different from an actual ventilation system, where the thermostat (or similar controller) is used to determine when the cold air should be supplied to the room (determined by the temperature setting on the thermostat).

5.3   HVAC Requirements

The standard temperature, relative humidity (rh), and airflow rates inside a room in an office building during winter and summer months are given in Table 5.1.

31

Design Conditions Inside A Room
(Adapted from the ASHRAE Handbook, 1995)

Office Buildings	Winter	Summer	Air Movement	Circulation, Air Changes per Hour
British Units	70 to 74° F 20 to 30% rh	74 to 78° F 50 to 60% rh	25 to 45 fpm 0.75 to 2 cfm/ft²	4 to 10
Metric Units	296.3 to 298.5 K	294.1 to 296.3 K	7.62 to 13.72 m/min 0.127 to 0.229 m/s	155.0 to 387.4 m³/hr

Table 5.1 Design conditions in a room [Howell, Ronald, and Saur, 1998]

5.4   Room 1: Ceiling Ventilation (VAV)

Figure 5.3 shows the schematic of Room 1 with two vents in the ceiling.

Grid (Time=3.0000e+02)   Aug 10, 2009
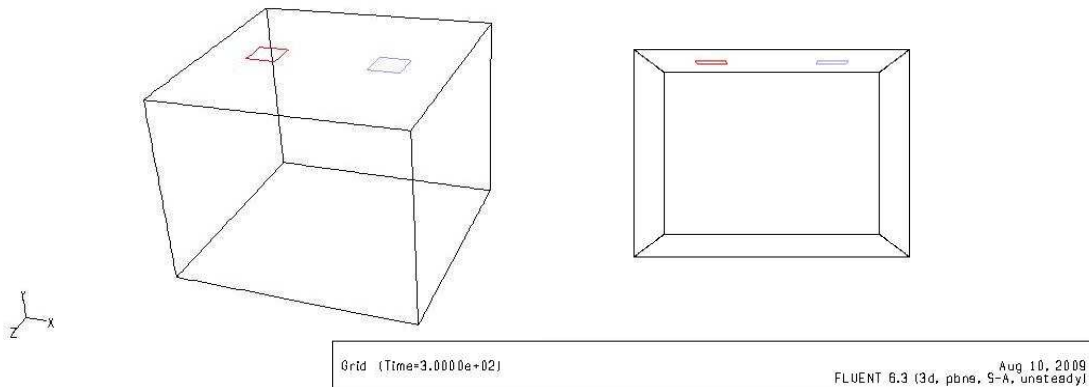   FLUENT 6.3 (3d, pbns, S-A, unsteady)

Figure 5.3 Room 1 geometry: 3-D view and the side View

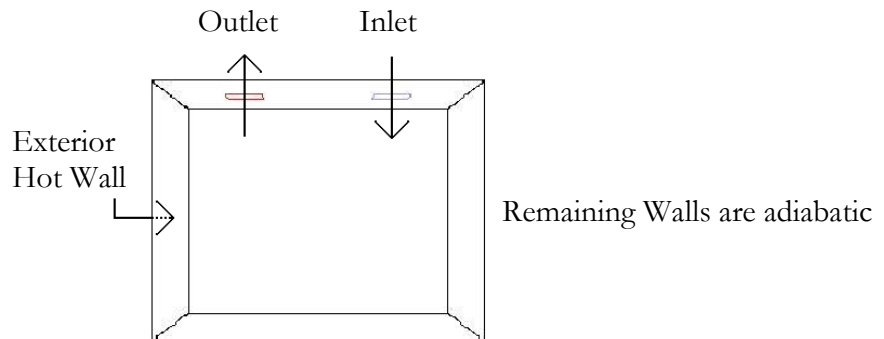Figure 5.4 shows the two vents in the ceilings and the boundary conditions as given in Table 5.2.

Figure 5.4 Room 1 boundary conditions

Room 1 Boundary Conditions

Boundary	Boundary Type	Settings	
Hot Wall	Isothermal	**Temp:**	80° F (299.817 K)
All Other Walls, Floor and Ceiling	Adiabatic	**q**	= 0
Inlet Vent	Mass Flow Inlet	**Flow Rate:** **Temp:** **Direction:**	0.052767 kg/s 60° F (288.706 K) Normal to boundary
Outlet Vent	Pressure Outlet	**Back Flow Temp:** **Direction:**	295 K Normal to boundary

Table 5.2 Room 1 boundary conditions

5.4.1   Determination of Vent Size

In determining the size of the vents, the HVAC requirements are carefully considered. For the ceiling ventilation shown in Figure 5.4, both the inlet and outlet dimensions of the vents are 1'- 6" x 1' – 6" (Figure 5.5), which gives an area of 2.25 ft² (0.209 m²) for each vent. Now, by meeting the guidelines of four air changes per hour [Howell, Ronald, & Saur, 1998] for a volume of 38.738 m³, this vent size gives a flow velocity of 40.54 ft/min (0.206 m/sec), which meets the HVAC requirement for air movement [Table 5.1].
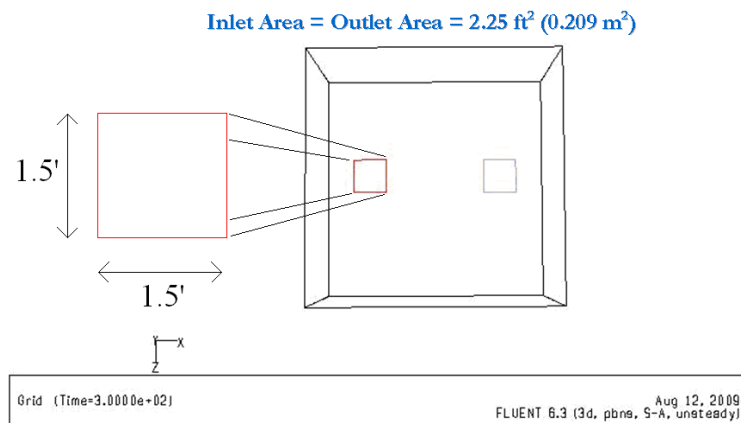

Figure 5.5 Room 1 vent sizes

5.4.2 Mesh Generation

3-D Cartesian mesh inside Room 1 was generated by GAMBIT, with a uniform grid spacing of 3" [Figure 5.6].
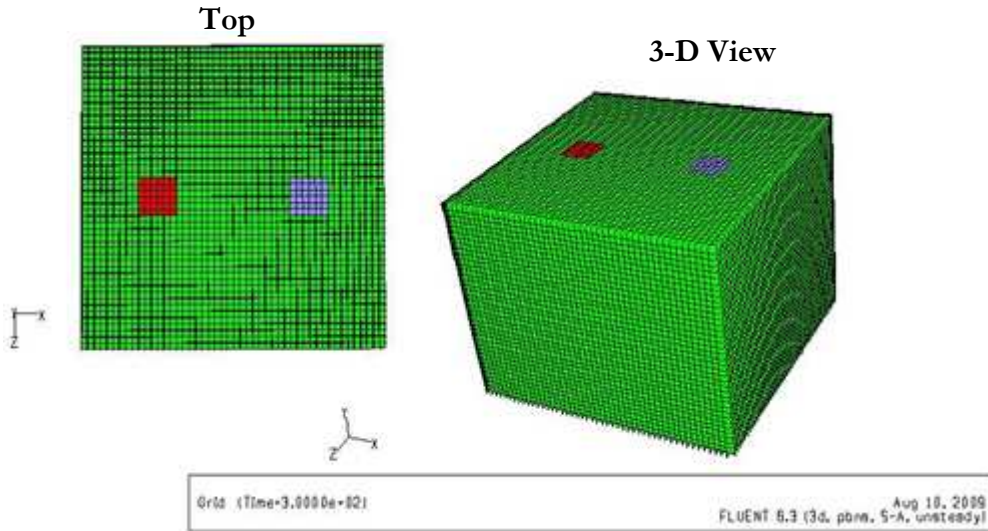

Figure 5.6 Room 1 mesh: top view and 3-D view

Despite the steep gradients near the walls, this spacing is sufficient to capture the flow field with reasonable accuracy [Madireddi, 2009]. This mesh has a cell count of 87,552 and a node count of 93,639.

5.4.3 Flow Field Computations

Many of the same parameters that were used in 2-D computations described in Chapter 4 are employed in the 3-D computations: Figure 4.2 is used to determine the variation of density with temperature, the initial starting values of temperature, T_0=288.16 K, and density, ρ_0= 1.225 kg/m^3, are employed, Discrete-ordinate method for the radiation calculation is employed, the governing equations are solved using the First-Order-Upwind scheme and the pressure is calculated using the PRESTO! scheme. However, the SIMPLE algorithm is employed for the coupling of the velocity and pressure instead of the PISO algorithm that was used in the 2-D computations. This change was done based on the recommendations of previous work in computing the natural convection flows [Tieszen,

Ooi, Burbin, & Behnia, 1998; Zhao, Zhang, Li, Yang, & Huang, 2003; Balaji, Hölling, & Herwig, 2007]. However, since the mesh is Cartesian (not skewed), there is little difference between the PISO and SIMPLE algorithms [Ansys Inc, 2007]. We also employed a different turbulence model, the Spalart Allmaras (S-A) instead of the k-ε (RNG) model that was used in the 2-D computations. The S-A is a simpler turbulence model, which only uses one equation to describe the turbulent eddy viscosity, compared to the k-ε (RNG) model, which uses two equations to calculate the eddy viscosity. All the three computations reported in Chapter 5 employ the S-A model.

5.4.4   Numerical Solution Procedure

To obtain the transient (time-varying) solution in the room for one cooling cycle of ninety minutes, the following numerical solution procedure is employed: The solution process is initialized using a steady state solution obtained with the boundary conditions on the wall given in Table 5.1 with vents closed. The unsteady solver is then run with vents open for a ten minute period using a constant time step[2] determined by the stability condition. After running the transient solution for ten minutes with vents open, the vents are closed and the transient solution is calculated for an additional eighty minutes.

5.4.5   Results and Analysis

Figure 5.7 shows various cross-sectional xy- and yz- planes where we show the temperature and velocity contours. The temperature contour plots (Figures 5.8-5.15), show the change in the room temperature progress with time in the yz-plane at z-50. It should be noted that at z-50 yz-plane intersects both the vents. The temperature scale (288 - 300 K) is the same in all the contour plots. It can be seen from these contours plots that the cold air jet exits the inlet vent for the first ten minutes slowly spreading inside the room (Figures 5.8 – 5.11). After the vent is closed after ten minutes into the ninety minute cooling cycle, the cold air jet starts mixing with the existing warm air in the room, thereby lowering the temperature of the

---

[2] To ensure stability, check that the time step $\Delta t \leq$ CFL condition [Ansys Inc, 2007].

room (Figures 5.12 - 5.13). The hot wall (80° F) continues to heat the room for the entire time period of 90 minutes. As a result, the temperature in the room begins to rise after 40 minutes or so. At the end of the 90 minute cooling cycle (Figure 5.15), the temperature of the room becomes close to that of the hot wall, 80° F (299.8 K). Figures 5.18 – 5.28 show the temperature contours in a 3-D domain; they show the areas of the room which are at cooler temperature (60 - 74° F). These contours depict the cold air jet exiting from the vent and extending to the floor after two and half minutes (Figure 5.18 & 5.19). As time progresses, the cold air continues to mix with air in the room and finally after ten minutes nearly the entire room is at temperatures between $60 – 74^0$ F (Figures 5.24 – 5.25). After ten minutes the vents are closed. Then, after twenty minutes, the top half of the room is at temperature $>74^0$ F (Figure 5.26 – 5.27), and after thirty minutes, the room is completely void of any air below 74° F (Figure 5.28). Note there is a small temperature gradient around the vents (Figure 5.28). These small traces of cold air near the vents are caused by the boundary conditions at the inlet and outlet vents. The mass flow rate for both the vents is zero; however, it is necessary to set a temperature boundary condition at the vents, which is set at the average volume temperature in the room after ten minutes (71.3° F).

The velocity magnitude contours (Figure 5.16) and velocity vectors (Figure 5.17) are shown in the yz-plane at z-50. From these figures, it can be seen that the column of cool air jet extends from the inlet to the floor in about 2.5 minutes. It can be observed that the jet velocity which is ~0.2 m/s at the inlet vent significantly increases to ~0.5 m/s near the middle of the room: this flow velocity first increases as the jet descends to the middle of the room and then decreases as it moves into the region of higher density cool air near the floor.

The change in the total energy of the fluid in a time period of 90 minutes is shown in Figure 5.29. It is directly monitored by FLUENT and is given in Joules per unit mass (J/kg). The unit of specific heat (C_p) is J/kg/K. Thus, dividing the energy/mass by the specific heat of air (1006.43 J/kg/K), the curve for change in the average volume temperature with time (Figure 5.30) is obtained. This average volume temperature is also monitored directly from FLUENT. Figure 5.30 shows that the average volume temperature of the room decreasing when the inlet vent is open for ten minutes and it starts increasing after the vent is closed after ten minutes eventually approaching the original room temperature after 90 minutes.
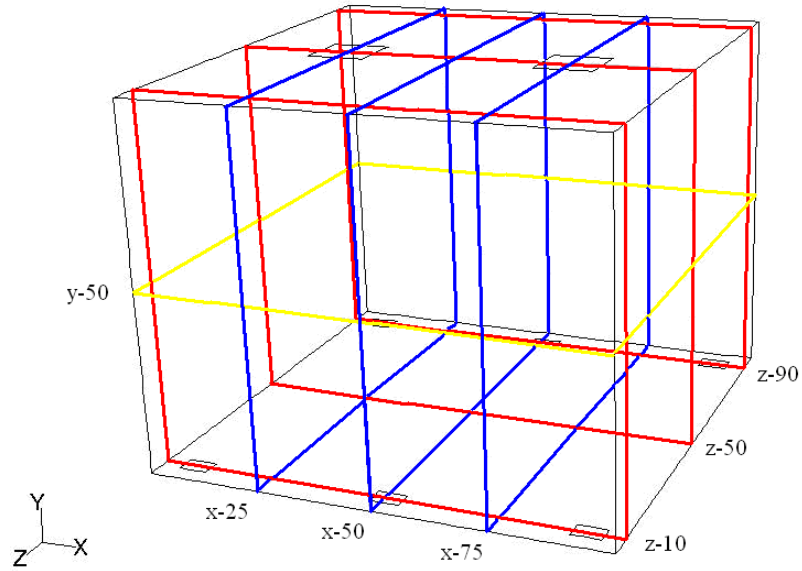
Grid Layout

Figure 5.7 Results for all three ventilation systems (Room 1, Room 2, and Room 3) are given in the xy- and yz-planes shown in this figure.

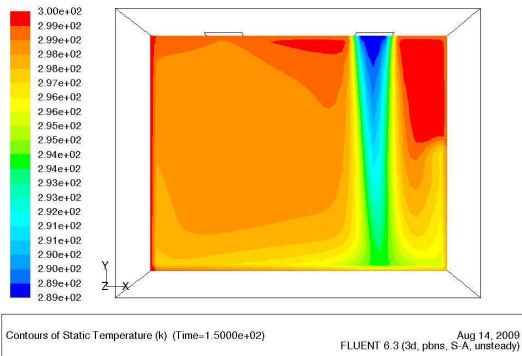## Temperature Contours in YZ-Plane at Z-50 with Flow On

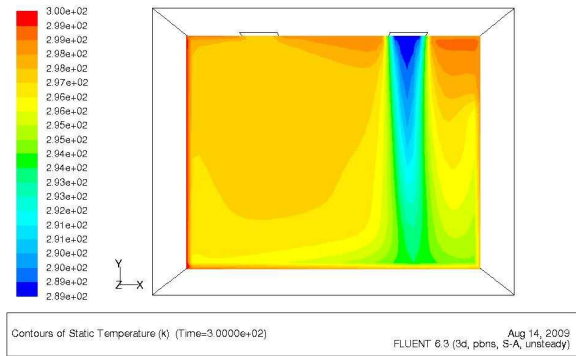**Figure 5.8 Temperature contours in the yz-plane at z-50 after 2.5 minutes (vents open - flow on)**

Figure 5.9 Temperature contours in the yz-plane at z-50 after 5 minutes (vents open - flow on)
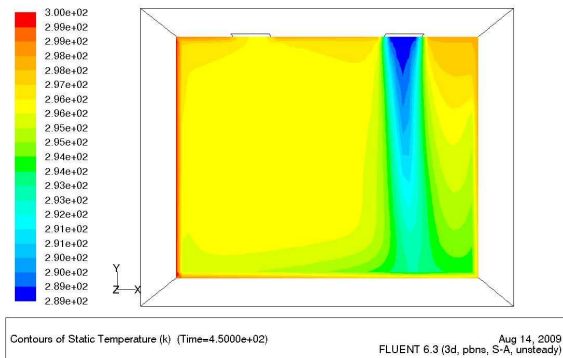

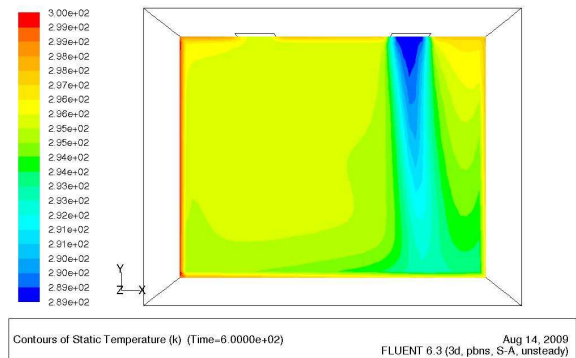**Figure 5.10 Temperature contours in the yz-plane at z-50 after 7.5 minutes (vents open - flow on)**

Figure 5.11 Temperature contours in the yz-plane at z-50 after 10 minutes (vents open - flow on)

37

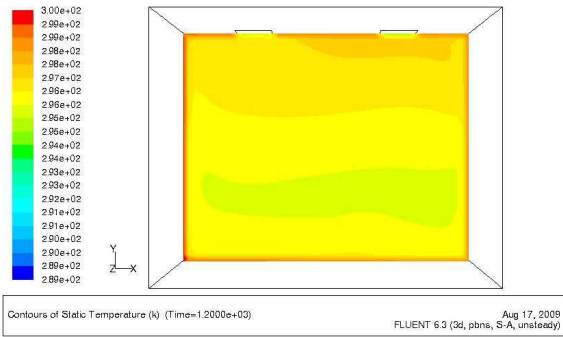# Temperature Contours in YZ-Place at Z-50 with Flow Off

Figure 5.12 Temperature contours in the yz-plane at z-50 after 20 minutes (vents open - flow on)
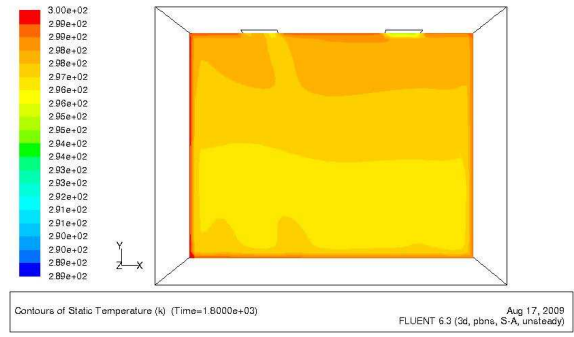

Figure 5.13 Temperature contours in the yz-plane at z-50 after 30 minutes (vents open - flow on)
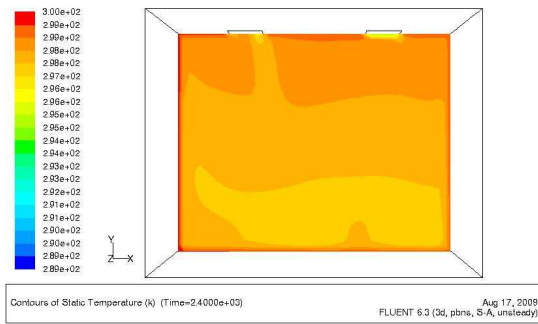

Figure 5.14 Temperature contours in the yz-plane at z-50 after 40 minutes (vents open - flow on)
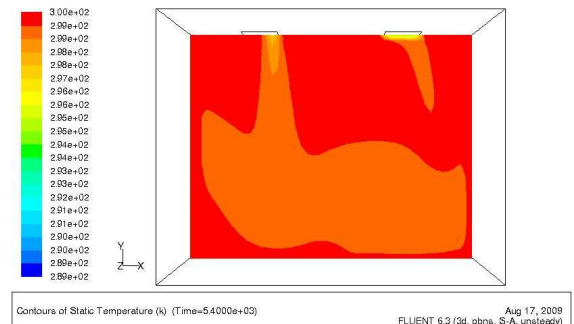

Figure 5.15 Temperature contours in the yz-plane at z-50 after 90 minutes (vents open - flow on)

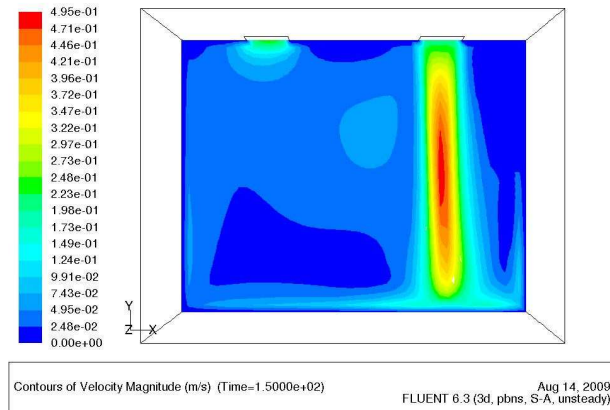# Velocity Magnitude Contours YZ-Plane at Z-50 with Flow On

Figure 5.16 Velocity Magnitude contours in yz-plane at z-50 after 2.5 minutes (vents open - flow on)

Velocity Vectors YZ-Plane at Z-50 with Flow On

Velocity Vectors Colored By Velocity Magnitude (m/s) (Time=1.5000e+02)   Aug 14, 2009
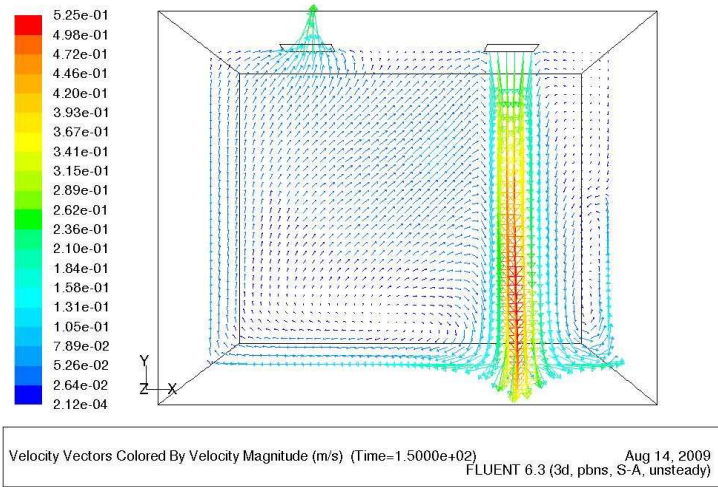FLUENT 6.3 (3d, pbns, S-A, unsteady)

Figure 5.17 Velocity vectors in yz-plane at z-50 after 2.5 minutes (vents open - flow on)

3-D Temperature Contours with Flow On (Temperature range is set from 60° to 74°F)
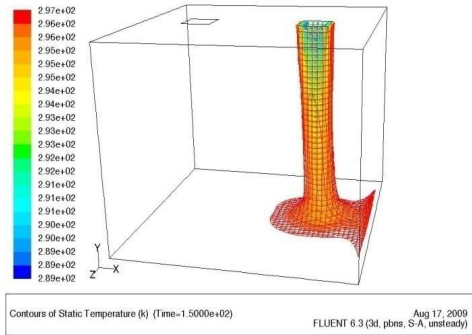## 2.5 Minutes (flow on)

Contours of Static Temperature (k) (Time=1.5000e+02)   Aug 17, 2009
FLUENT 6.3 (3d, pbns, S-A, unsteady)

Contours of Static Temperature (k) (Time=1.5000e+02)   Aug 17, 2009
FLUENT 6.3 (3d, pbns, S-A, unsteady)

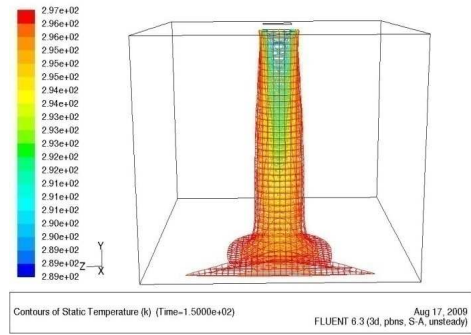**Figure 5.18 3-D temperature contours after 2.5 minutes: view 1**

Figure 5.19 3-D temperature contours after 2.5 minutes: view 2
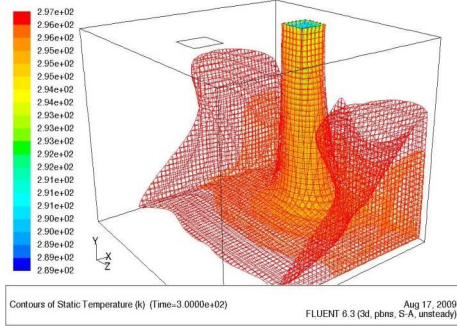
5 Minutes (flow on)

Figure 5.20 3-D temperature contours after 5 minutes: view 1

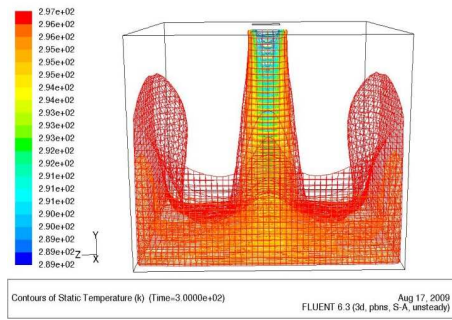**Figure 5.21 3-D temperature contours after 5 minutes: view 2**
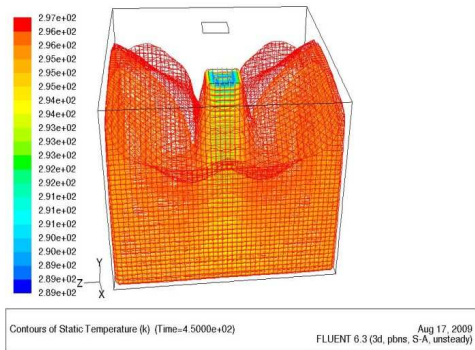
7.5 Minutes (flow on)

Figure 5.22 3-D temperature contours after 7.5 minutes: view 1

Figure 5.23 3-D temperature contours after 7.5 minutes: view 2

10 Minutes (flow on)

Figure 5.24 3-D temperature contours after 10 minutes: view 1

Figure 5.25 3-D temperature contours along z-50 after 10 minutes: view 2

3-D Temperature Contours with Flow Off (Temperature range is set from 60° to 74°F)
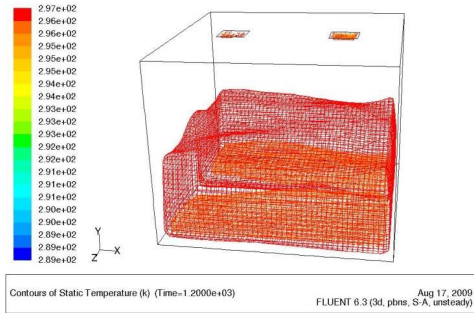
20 Minutes (flow off)

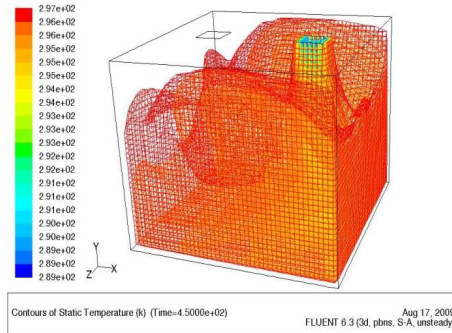**Figure 5.26 3-D temperature contours after 20 minutes: view 1**
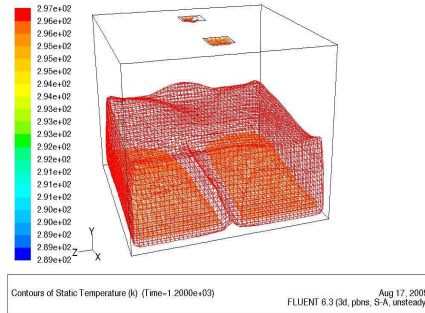
Figure 5.27 3-D temperature contours after 20 minutes: view 2
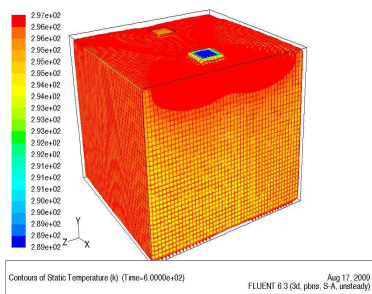
30 Minutes (flow off)
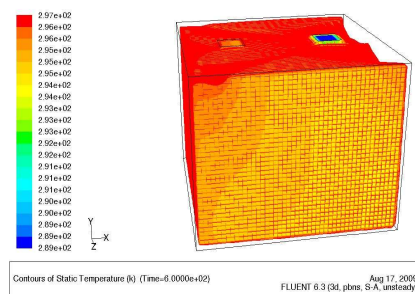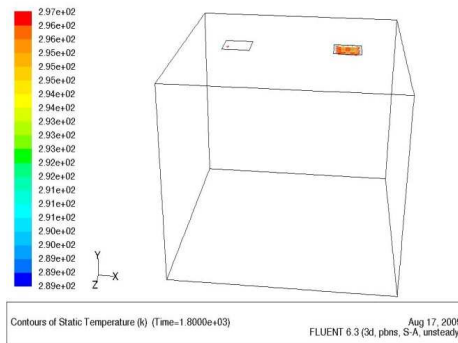

Figure 5.28 3-D temperature contours after 30 minutes
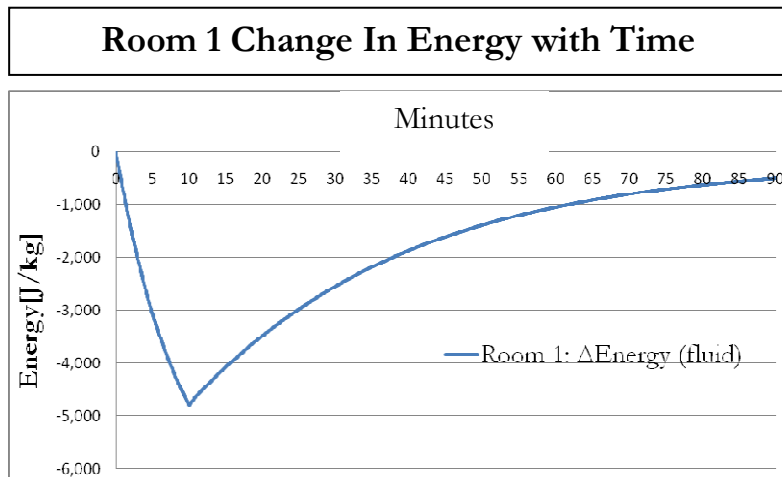
Figure 5.29 Room 1 change in energy with time
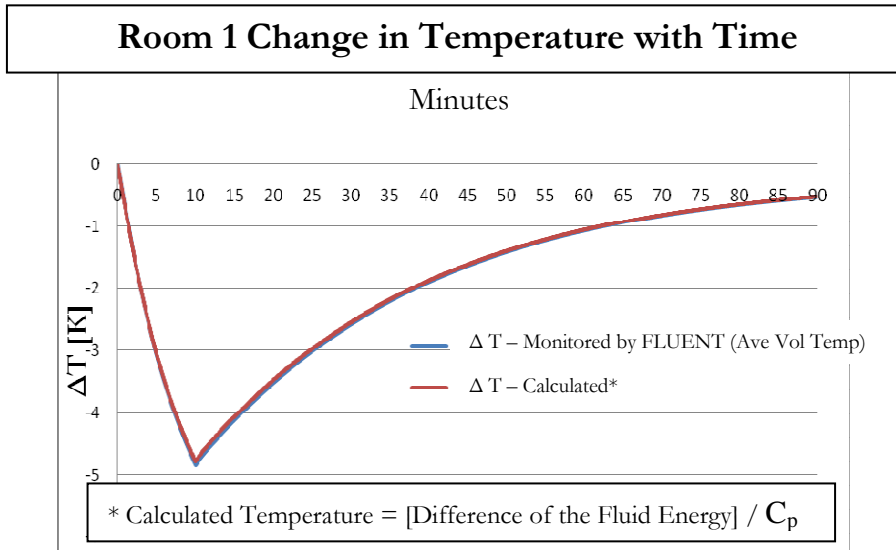
Figure 5.30 Room 1 change in temperature with time

5.5   Room 2: Displacement Ventilation

Figure 5.31 shows the schematic of Room 2 with the two outlet vents in the ceiling and six inlet vents on the floor.

Total Outlet Area = 4.5 ft^2 (0.418 m^2)
Total Inlet Area = 2.25 ft^2 (0.209 m^2)
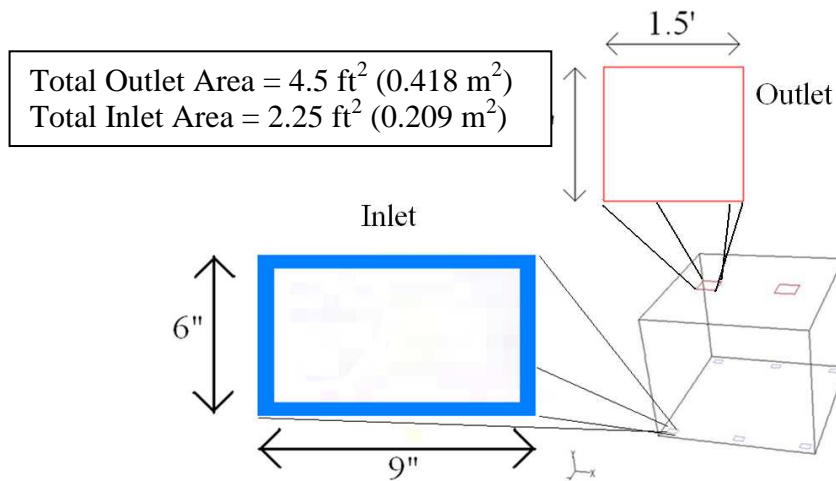
Figure 5.31 Room 2 vent sizes in the ceiling and the floor

5.5.1   Determination of Vent Sizes

Room 2 inlet vents are designed to have the same total inlet vent area as Room 1. There are six inlet vents on the floor. Hence, the Room 2 inlet vents are 6" x 9", which gives an area of

2.25 ft^2 (0.209 m^2) for six vents (Figure 5.31). Since there is no change in the total inlet vents area compared to Room 1, Room 2 meets the ASHRAE guidelines of air movement (Section 5.4.1) in the room. The six inlet vents are placed on the floor near the adiabatic walls. This is done to keep the installation of the vents on the floor practical, so that the vents may not blocked by the furniture in the room. The outlet vent area of Room 2 is double the size of the outlet vent area of Room 1. Each outlet vent is of the size, 1'-6" x 1-6", giving an area of 4.5 ft^2 (0.418 m^2)) for the 2 outlet vents in Room 2. The boundary conditions for Room 2 are given in Table 5.3.

Room 2 Boundary Conditions

| Boundary	Boundary Type	Settings	
Hot Wall	Isothermal Wall	**Temp:**	80° F (299.817 K)
All Other Walls, Floor and Ceiling	Adiabatic Wall	**q**	= 0
Inlet Vents (x 6)	Mass Flow Inlet	**Flow Rate:**	0.0087945 kg/s (=[0.052767 kg/s] / 6 vents)
		Temp:	60° F (288.706 K)
		Direction:	Normal to boundary
Outlet Vents (x 2)	Pressure Outlet	**Back Flow Temp:**	295 K
		Direction:	Normal to boundary

Table 5.3 Room 2 boundary conditions

5.5.2 Mesh Generation

The same 3-D Cartesian mesh that was employed for Room 1 is employed for Room 2 (Section 5.4.2). The mesh was generated by GAMBIT, with a uniform grid spacing of 3" (Figure 5.32).
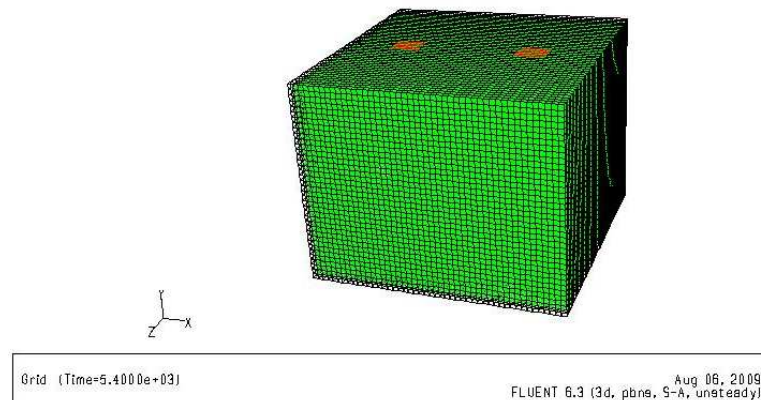

Grid (Time=5.4000e+03)   Aug 06, 2009
                                                        FLUENT 6.3 (3d, pbns, S-A, unsteady)

Figure 5.32 Room 2 mesh: 3-D view

43

5.5.3   Flow Field Computations

The same flow field computation methodology that was employed for Room 1 (Sections 5.4.3 & 5.4.4) is employed for Room 2.

5.5.4   Results and Analysis

Figure 5.33 shows various cross-sectional xy- and yz-planes where we show the temperature and velocity contours. The temperature contour plots (Figures 5.33-5.5.40) show the change in the room temperature with time in the yz-plane at z-50. Note that at z-50, yz-plane intersects both of the ceiling vents. The temperature scale (288 - 300 K) is the same in all the contour plots. The contour plots with the flow on (Figures 5.33 - 5. 36) clearly show the two layer thermal stratification associated with DV [Linden, 1999]. This two layer thermal stratification forms because of the effects of buoyancy on the fluid. The higher density cold air from the vents settles on the floor and displaces the lower density hot air at the ceiling. Over time, the cold air mixes with the convective heat from the hot wall and warmer air already present in the room, and in doing so a more gradual change from the ambient conditions at the bottom of the enclosure to a maximum temperature at the top is observed [Linden, 1999](Figure 5.36). After the vents are closed, ten minutes into the cycle, the cold air near the floor continues to mix with the existing warm air in the room, thereby diminishing the temperature gradients (Figures 5.37 - 5.40). It is apparent that the DV system is designed to flush out the lower density warm air, which when compared to the mixing demonstrated in Room 1, not only more effectively cools the room but also more effectively removes the contaminants in the air [Linden, 1999]. Similar to Room 1, the hot wall (80^0 F) continues to heat the room for the entire time period of 90 minutes. As a result, the temperature in the room continues to rise after 40 minutes or so (Figure 4.39). At the end of the 90 minute cooling cycle (Figure 5.40), the temperature of the room becomes close to that of the hot wall, 80^0 F (299.8 K).

Figures 5.43 - 5.52 show the temperature contours in a 3-D domain; similarly to Room 1, they show the areas of the room which are at cooler temperature (60 - 74^0 F). These contours depict the two-layer thermal stratification extending for the length of the room

44

(Figures 5.43 - 5.49). As time progresses, the cold air continues to mix with the air in the room and finally after ten minutes, all of the air except for a small portion near the ceiling is at temperatures between 60 - 74^0 F (Figure 5.49). After ten minutes, the vents are closed. Then, after twenty minutes, much of the room is still at temperature <74^0 F (Figure 5.50). After thirty minutes, only the bottom one-third portion of the room is at temperature <74^0 (Figure 5.51), and finally after forty minutes, the room is completely void of any air below 74^0 F (Figure 5.52). The small temperature gradients around the vents (Figure 5.52) are an artifact of the boundary conditions as explained in Section 5.4.5.

The velocity magnitude contours after two and half minutes, Figures 5.41 and 5.42, are shown in the yz-plane at z-10 and z-50 respectively. From these contours, we notice the significant air movement near the floor, which is a characteristic of DV systems.

The change in temperature in a time period of 90 minutes is shown in Figure 5.53. As explained in Section 5.4.5, temperature change from the average volume temperature is directly monitored from FLUENT while the temperature difference is calculated by dividing the change in the total energy of the fluid, given in energy per unit mass, by the C_p. Note that the total energy of the fluid is directly monitored by FLUENT. Figure 5.53 shows that the average volume temperature of the room decreases when the inlet vents are open for ten minutes and it starts increasing after the inlet vents are closed after ten minutes eventually approaching the original room temperature after 90 minutes.

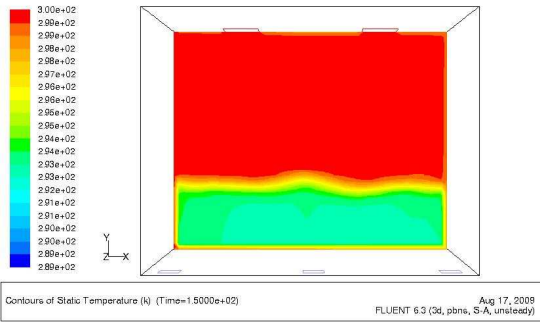# Temperature Contours in YZ- Plane at Z-50 with Flow On

Figure 5.33 Temperature contours in the yz-plane at z-50 after 2.5 minutes (vents open - flow on)
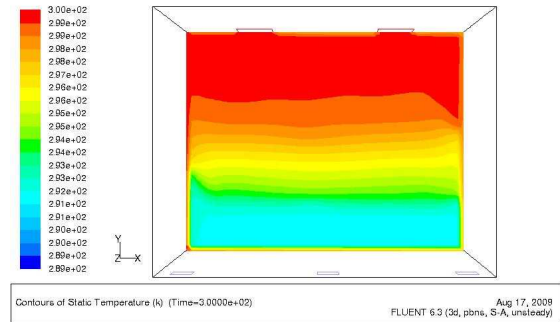

Figure 5.34 Temperature contours in the yz-plane at z-50 after 5 minutes (vents open - flow on)
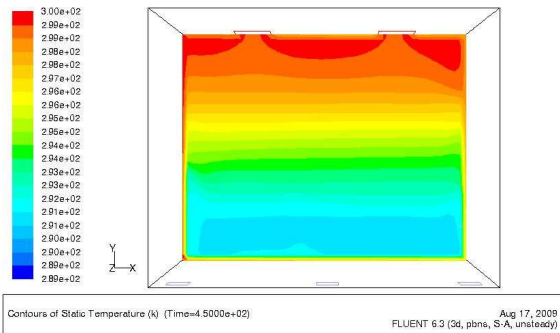

Figure 5.35 Temperature contours in the yz-plane at z-50 after 7.5 minutes (vents open - flow on)
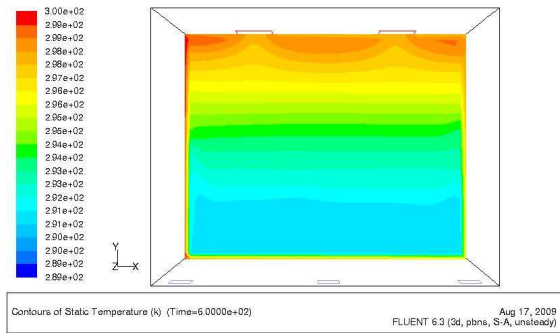

Figure 5.36 Temperature contours in the yz-plane at z-50 after 10 minutes (vents open - flow on)

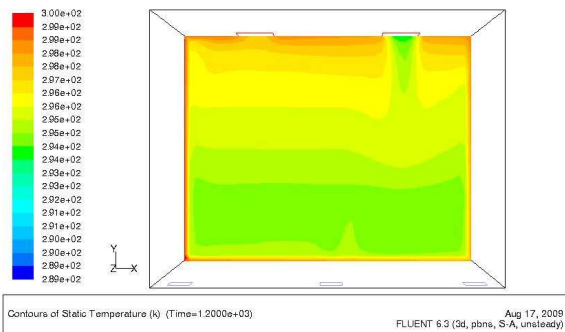# Temperature Contours in YZ- Plane at Z-50 with Flow Off

Figure 5.37 Temperature contours in the yz-plane at z-50 after 20 minutes (vents closed - flow off)
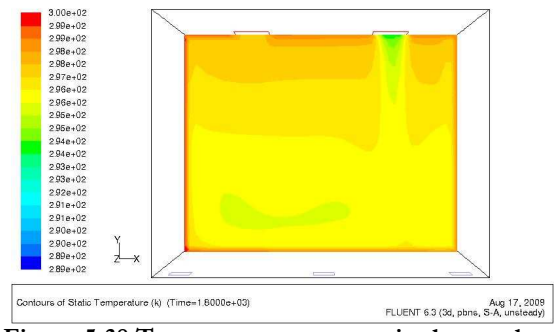

Figure 5.38 Temperature contours in the yz-plane at z-50 after 30 minutes (vents closed - flow off)
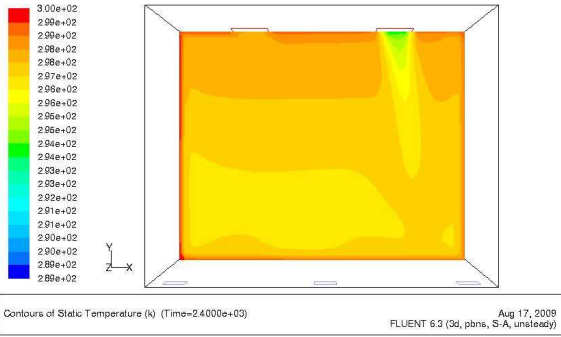
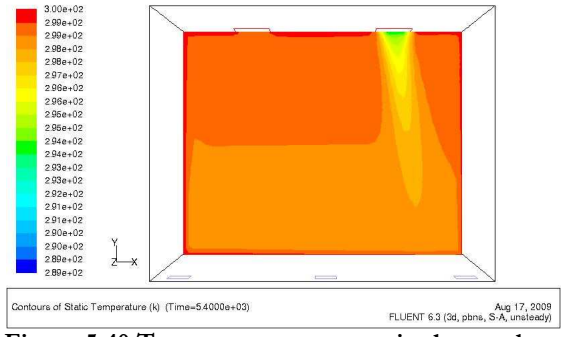**Figure 5.39 Temperature contours in the yz-plane at z-50 after 40 minutes (vents closed - flow off)**

Figure 5.40 Temperature contours in the yz-plane at z-50 after 90 minutes (vents closed - flow off)

Velocity Magnitude Contours in YZ-Plane after 10 Minutes with Flow On
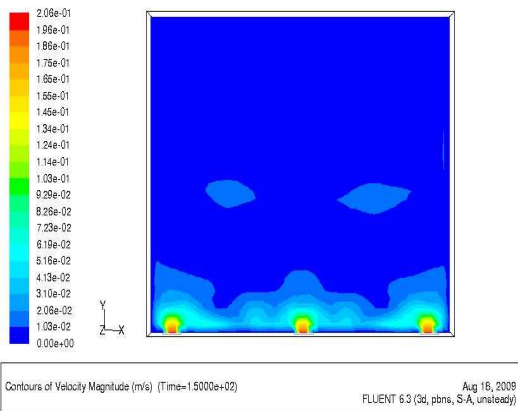
Figure 5.41 Velocity magnitude contours in the yz-plane at z-10 after 2.5 minutes (vents open - flow on)
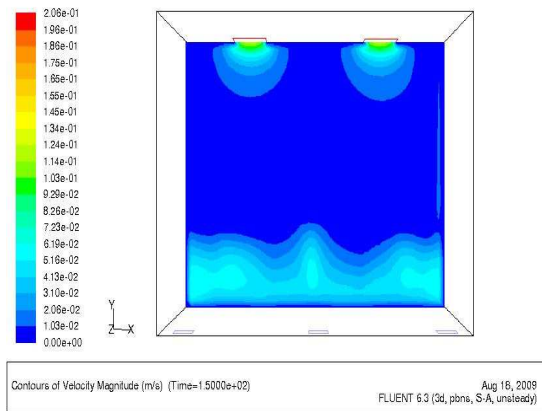
Figure 5.42 Velocity magnitude contours in yz-plane at z-50 after 2.5 minutes (vents open - flow on)

3-D Temperature Contours with Flow On
(Temperature range is set from 60° to 74°F)

2.5 Minutes (flow on)

Figure 5.43 3-D temperature contours after 2.5 minutes: view 1

Figure 5.44 3-D temperature contours after 2.5 minutes: view 2

47

5 Minutes (flow on)

Figure 5.45 3-D temperature contours after 5 minutes: view 1

Figure 5.46 3-D temperature contours after 5 minutes: view 2

7.5 Minutes (flow on)

Figure 5.47 3-D temperature contours after 7.5 minutes: view 1

Figure 5.48 3-D temperature contours after 7.5 minutes: view 2

10 Minutes (flow on)
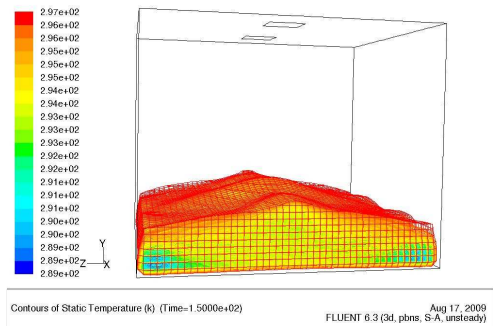

Figure 5.49 3-D temperature contours after 10 minutes: view 1

3-D Temperature Contours with Flow Off
(Temperature range is set from 60° to 74°F)
20 Minutes (flow off)
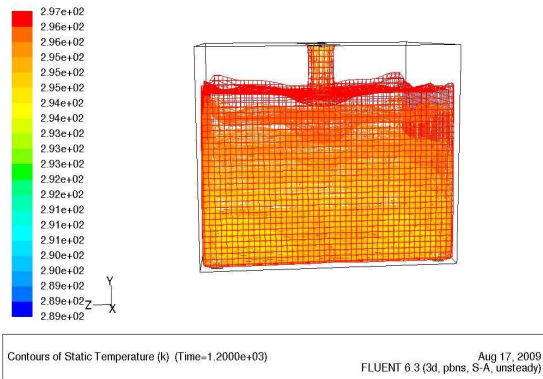
Figure 5.50 3-D temperature contours after 20 minutes: view 1
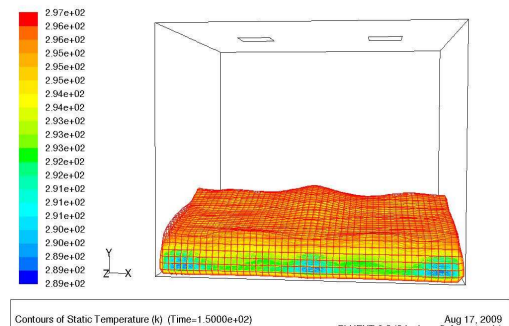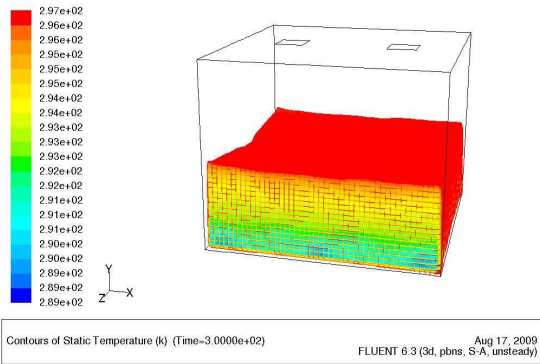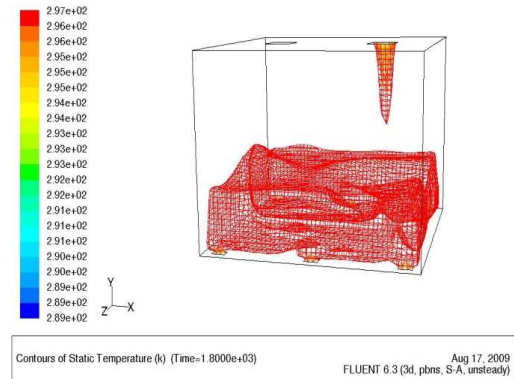

Figure 5.51 3-D temperature contours after 30 minutes: view 2

30 Minutes (flow off)
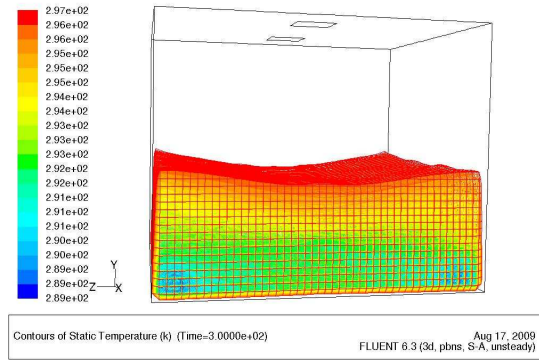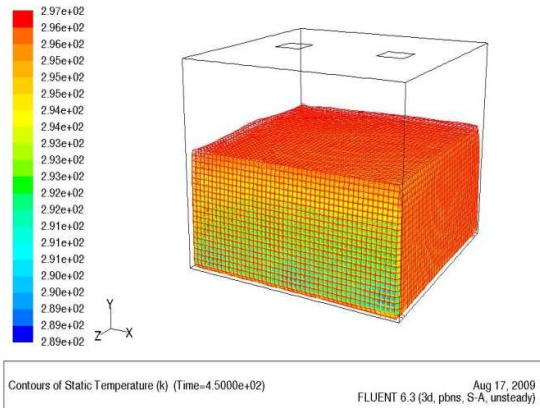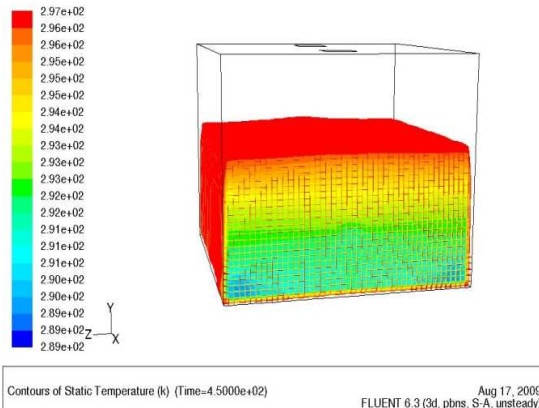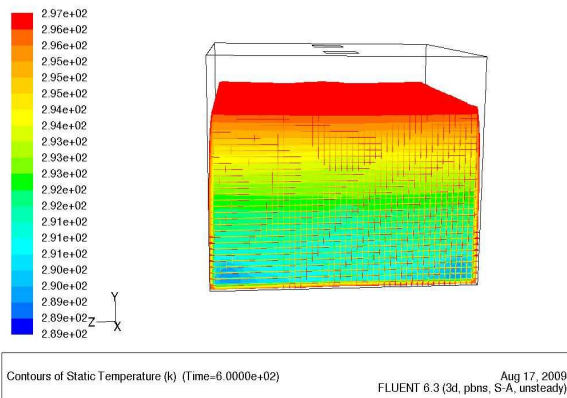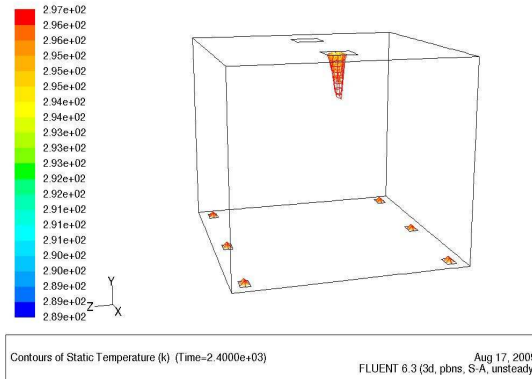

Figure 5.52 3-D temperature contours after 30 minutes
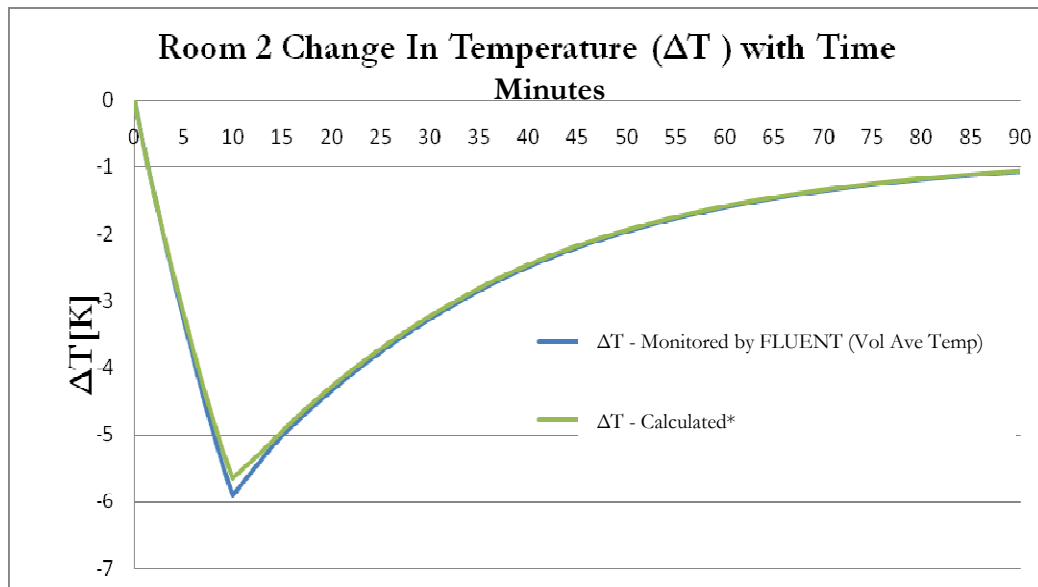
Figure 5.53 Room 2 change in temperature with time

49

5.6   Room 3: Displacement Ventilation with Chilled Ceiling

Figure 5.54 shows the schematic of Room 3 with the outlet vent placed along the adiabatic wall near the floor (opposite to the hot wall), the six inlet vents placed on the floor near the side walls, and the radiation slab placed close to the ceiling.
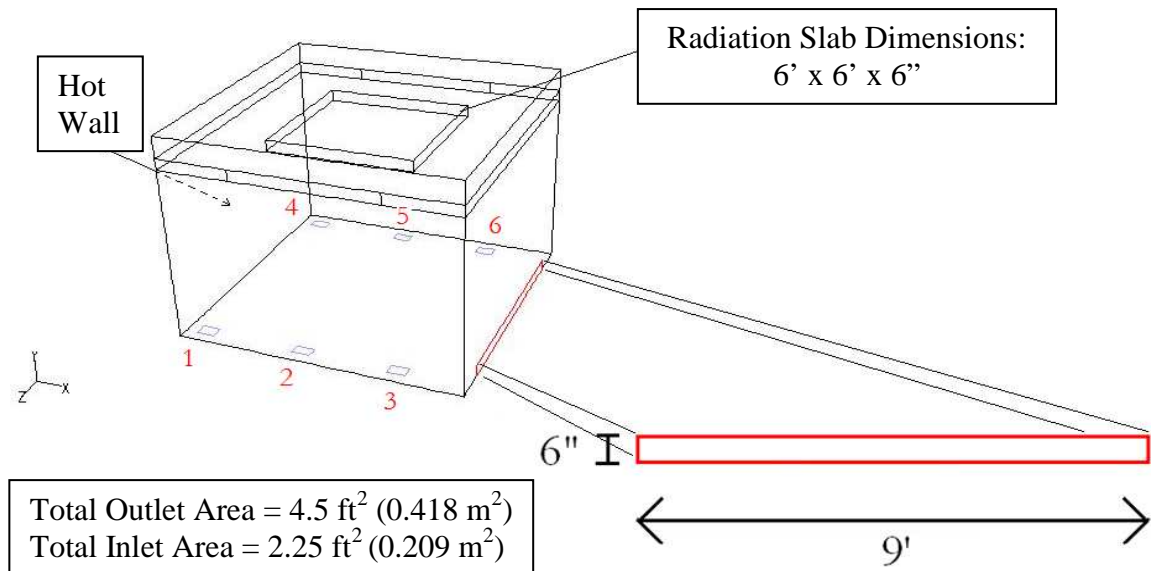
Figure 5.54 Room 3 geometry

5.6.1   Determination of Vent and Radiation Slab Sizes

For Room 3, there are no changes in the sizes of the inlet vents from Room 2, but there is a slight decrease in the volume (38.228 m^3) of Room 3 due to the radiation slab. By meeting the ASHRAE guidelines of four air changes per hour for this volume, these vent sizes (with a total area of 2.25 ft^2) give a flow velocity of 40.53 ft/min (0.203 m/sec), which meets the HVAC guidelines for air movement (Table 5.1). The outlet vent (6" x 9') is placed along the floor of the adiabatic wall opposite to the hot wall. This gives an area of 4.5 ft^2 (0.418 m^2), which is the same as that for Room 2. Room 3 has the addition of the radiation slab, 6' x 6' x

50

6", which provides the chilled ceiling effect. The radiation slab is placed 6" below the ceiling[3] in the center of the room.

The boundary conditions for this room are given in Table 5.4. The radiation slab is treated as a radiating wall at 60° F (288.706 K) with an emissivity of 0.85 (~weathered stainless steel). Notice that the outlet vent is moved from the ceiling to the base of the wall (Figure 5.54), which puts it in close proximity to inlet vents labeled as three and six in Figure 5.54. Consequently, the flow from both of these inlet vents is directed at a 45° angle in the negative x-direction to keep the cold air from being directly discharged by the outlet vent. Otherwise, the boundary conditions are the same as for the previous Rooms 1 and 2 (Table 5.4).

Room 3 Boundary Conditions

Boundary	Boundary Type	Settings	
Hot Wall	Isothermal Wall	**Temp:**	80º F (299.817 K)
Radiation Slab	Radiating Wall	**Temp:**	60º F (288.706 K)
		Emissivity:	0.85 (~ weathered stainless steel)
All Other Walls, Floor and Ceiling	Adiabatic Wall	**q**	= 0
Inlet Vents	Mass Flow Inlet	**Flow Rate:**	0.0087945 kg/s (= [0.052767 kg/s] / 6 vents)
		Temp:	60º F (288.706 K)
		Direction:	Vents 1,2,4,5 - Normal to boundary Vents 3,6 - 45° (-)x direction
Outlet Vent	Pressure Outlet	**Back Flow Temp:**	295 K
		Direction:	Normal to boundary

Table 5.4 Room 3 Boundary Conditions

5.6.2   Mesh Generation

Similar to Rooms 1 and 2, a 3-D Cartesian mesh inside Room 3 was generated by GAMBIT, with a uniform grid spacing of 3" (Figure 5.55).

---

[3] This design is close to reality since often times, when retrofitting existing buildings with a hydronic system, radiant panels are simply added to the ceiling rather than by totally stripping the existing framework, which generally is not cost effective.
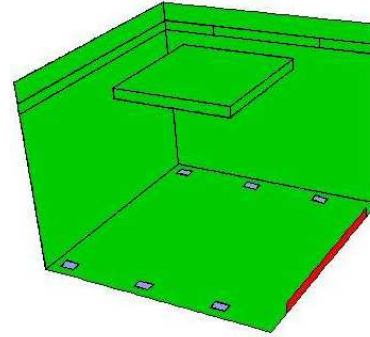
Figure 5.55 Room 3 mesh: 3-D view   **Figure 5.56 Room 3 interior view**

The Room 3 mesh varies slightly from the other two rooms, since the radiation slab is included in Room 3. Consequently the volume for Room 3 also slightly smaller than the other two rooms (Room 3 Volume = 38.228 m^3). This mesh has a cell count of 86,400 and a node count of 93,110.

5.6.3   Flow Field Computations

The same flow field computation methodology that was employed for Rooms 1 and 2 (Sections 5.4.3 & 5.4.4) is employed here for the solution of Room 3. The radiation boundary condition on the slab is included in this simulation.

5.6.4   Results and Analysis

Figure 5.57 shows various cross-sectional xy- and yz-planes where we show the temperature and velocity contours. The temperature contour plots (Figures 5.57-5.5.64) show the change in the room temperature with time in the yz-plane at z-50. Note that at z-50, yz-plane intersects the center of the radiation slab near the ceiling. The temperature scale (288 - 300 K) is the same in all the contour plots. The contour plots with the flow on (Figures 5.57-5.60) show the gradual cooling of the room. By ten minutes (Figure 5.60), the room temperature is uniformly cool with very little temperature variation. After the inlet floor vents are closed, ten minutes into the cycle, we observe that the hot wall is gradually heating the room (Figures 5.61-5.64). Similar to the other two rooms (Rooms 1 & 2), the hot wall (80^0 F) continues to heat the room for the entire time period of 90 minutes; however,

52

because the radiation slab continues to operate for the 90 minute cycle, the Room 3 temperature remains relatively cooler throughout the simulation.

Figures 5.67 - 5.79 show the temperature contours in a 3-D domain; similarly to the other two rooms, they show the areas of the room which are at cooler temperature (60 - 74^0 F). These contours depict the cold air jets exiting the inlet vents on the floor and diffusing near the corner of the hot wall and the ceiling (Figures 5.67 - 5.69). As time progresses, the cold air continues to mix with the air in the room and finally after ten minutes, nearly all the air inside the room is at temperatures between 60 - 74^0 F (Figure 5.74). After ten minutes, the vents are closed. Then, after twenty minutes, there are slightly higher temperatures near the walls, however much of core area of the room is still at temperatures <74^0 F (Figures 5.75- 5.77). Even after 90 minutes (Figure 5.79), large portions of the room are at ≤74^0 F. This is in stark contrast to the temperatures in the other two rooms (Rooms 1 &2), which after 90 minutes attain the temperature of the hot wall, 80^0 F (299.8 K).

The velocity magnitude contours, Figures 5.41 and 5.42, are shown after two and half minutes. Figure 5.41, shown in the yz-plane at z-10, illustrates the flow from the inlet vents along the floor. Note that vents 1, 2, and 3 are labeled in red. Also from this figure, note that vent 3 is at an angle of 45^0 in the negative x-direction. In figure 5.42, the 3-D velocity magnitude contours, show air jets extending from the inlet vents and some air movement in the center of the room.

The change in temperature in a time period of 90 minutes is shown in Figure 5.80. As explained in Section 5.4.5, the average volume temperature is directly monitored from FLUENT. Figure 5.80 shows that the average volume temperature of the room decreases when the inlet vents are open for ten minutes and it starts gradually increasing after the vents are closed after ten minutes. Unlike the other two rooms which nearly reach the temperature of the hot wall after 90 minutes, Room 3 continues to stay relatively colder with only a small increase in temperature by the end of the 90 minutes.

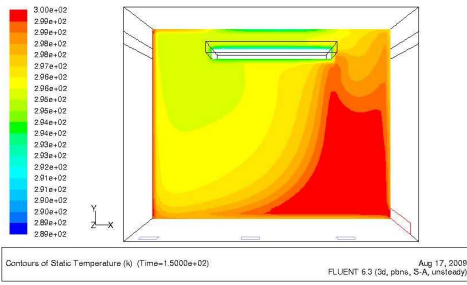# Temperature Contours in YZ-Plane at Z-50 with Flow On

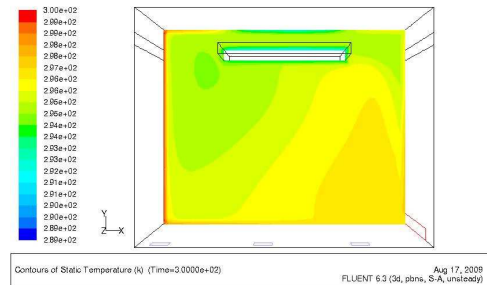**Figure 5.57 Temperature contours in yz-plane at z-50 after 2.5 minutes (vents open -flow on)**

Figure 5.58 Temperature contours in yz-plane at z-50 after 5 minutes (vents open -flow on)

Figure 5.59 Temperature contours in yz-plane at z-50 after 7.5 minutes (vents open -flow on)

Figure 5.60 Temperature contours in yz-plane at z-50 after 10 minutes (vents open -flow on)

Temperature Contours in YZ-Plane at Z-50 with Flow Off

Figure 5.61 Temperature contours in yz-plane at z-50 after 20 minutes (vents closed -flow off)
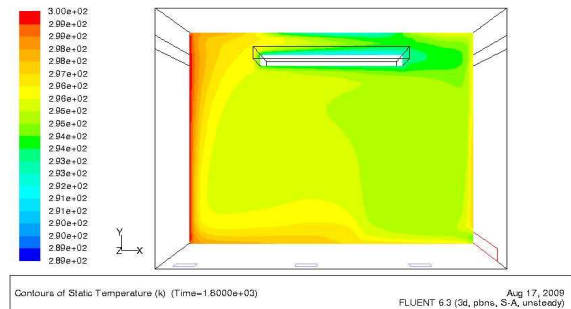
Figure 5.62 Temperature contours in yz-plane at z-50 after 30 minutes (vents closed -flow off)
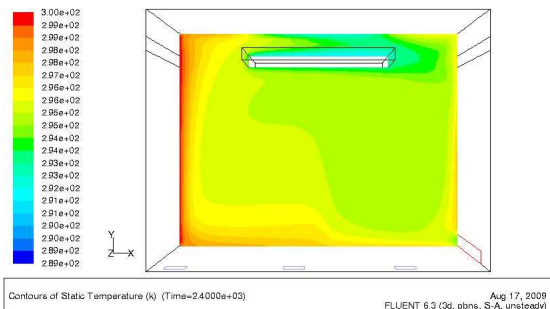
Figure 5.63 Temperature contours in yz-plane at z-50 after 40 minutes (vents closed -flow off)
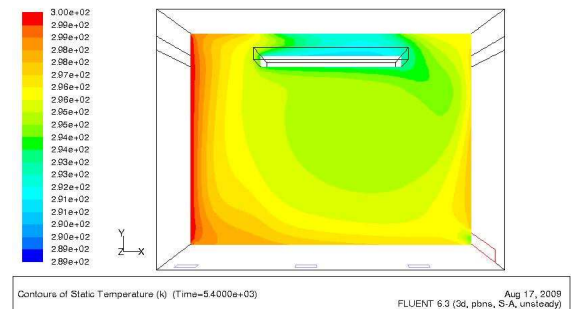
Figure 5.64 Temperature contours in yz-plane at z-50 after 90 minutes (vents closed -flow off)
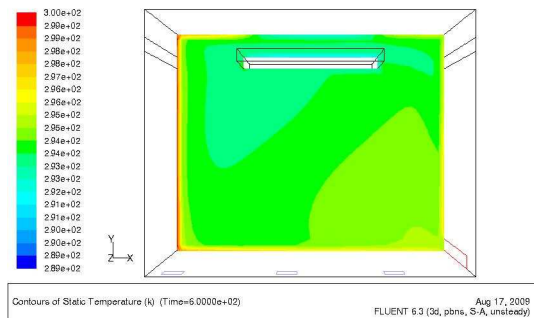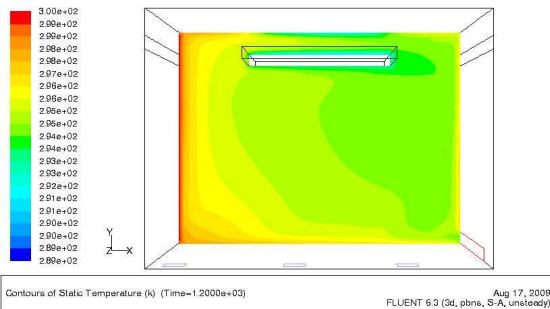
54

Velocity Magnitude Contours at 2.5 Minutes
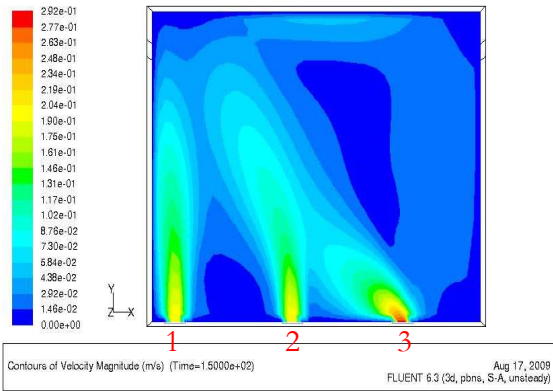
Figure 5.65 Velocity magnitude contours in yz-plane at Z-2.5 after 2.5 minutes
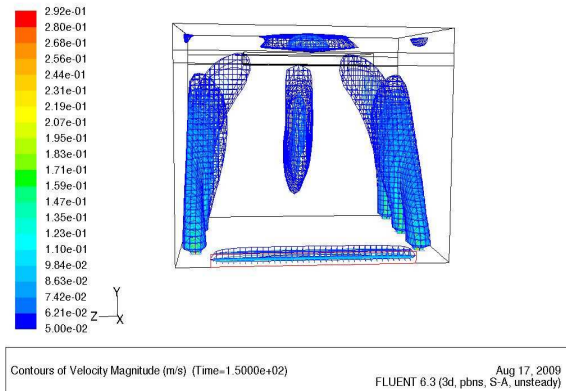
Figure 5.66 3-D velocity magnitude contours after 2.5 minutes

3-D Temperature Contours with Flow On
(Temperature range is set from 60° to 74°F)
2.5 Minutes (flow on)
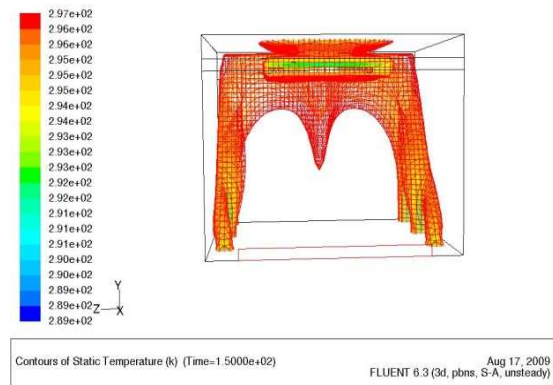
Figure 5.67 3-D temperature contours after 2.5 minutes: view 1
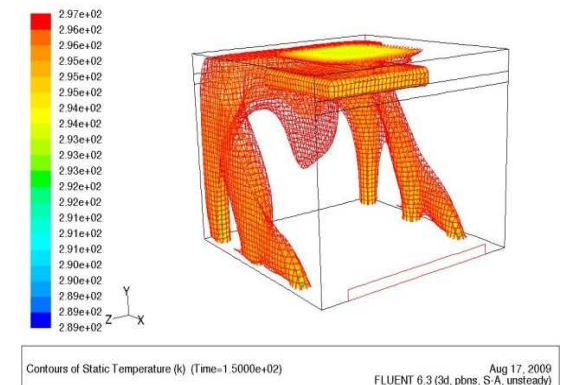
Figure 5.68 3-D temperature contours after 2.5 minutes: view 2
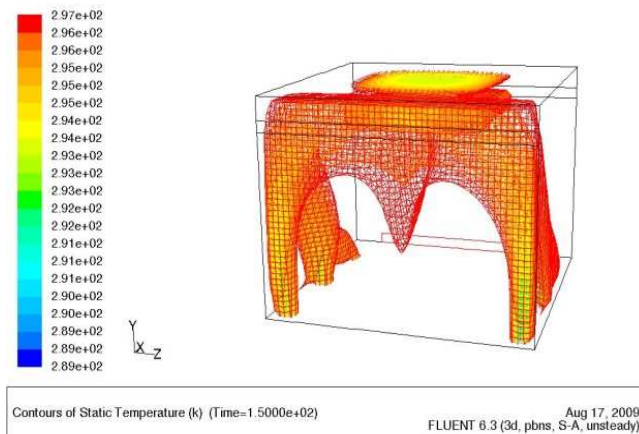
Figure 5.69 3-D temperature contours after 2.5 minutes: view 3

5 Minutes (flow on)
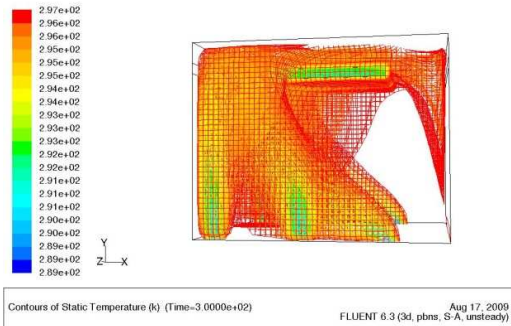
Figure 5.70 3-D temperature contours after 5 minutes: view 1
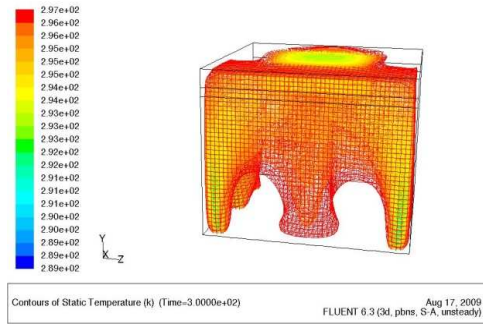
Figure 5.71 3-D temperature contours after 5 minutes: view 2
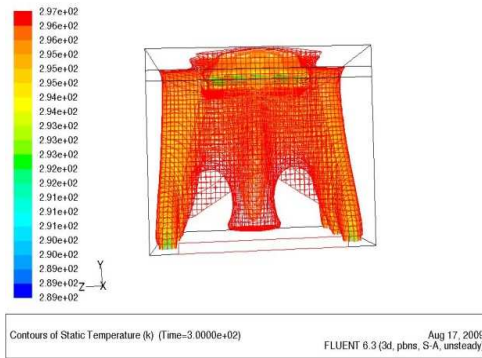
Figure 5.72 3-D temperature contours after 5 minutes: view 3

7.5 Minutes (flow on)
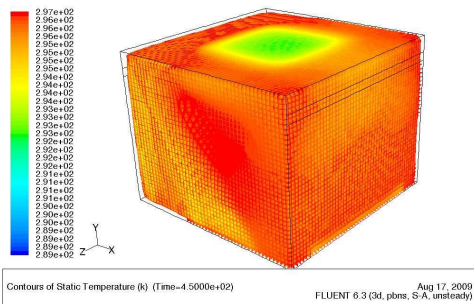
Figure 5.73 3-D temperature contours after 7.5 minutes: view 1

10 Minutes (flow on)

Figure 5.74 3-D temperature contours after 10 minutes: view 1

3-D Temperature Contours with Flow Off
(Temperature range is set from 60° to 74°F)
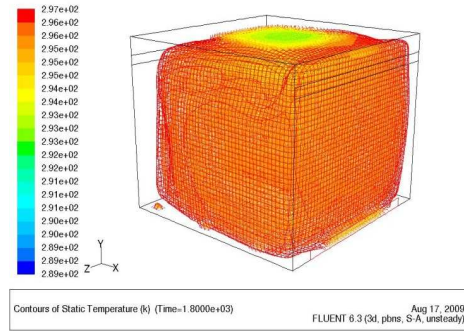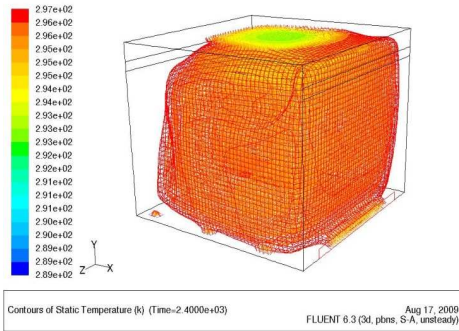
20 Minutes (flow off)

Figure 5.75 3-D temperature contours after 20 minutes

30 Minutes (flow off)

Figure 5.76 3-D temperature contours after 30 minutes

50 Minutes (flow off)
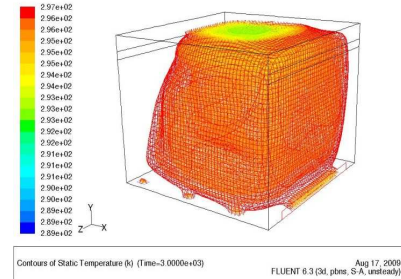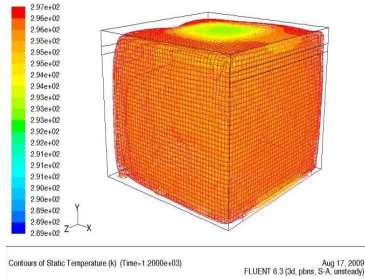
Figure 5.77 3-D temperature contours after 50 minutes

60 Minutes (flow off)

Figure 5.78 3-D temperature contours after 60 minutes

90 Minutes (flow off)
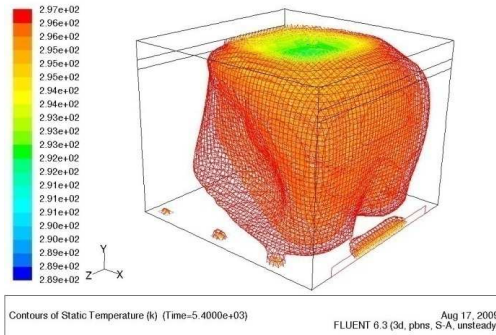
Figure 5.79 3-D temperature contours after 90 minutes

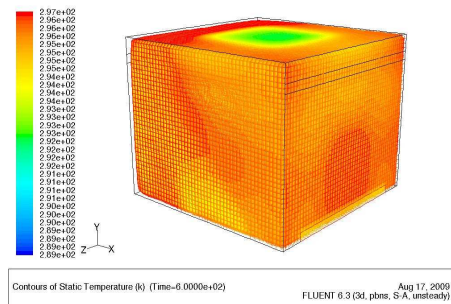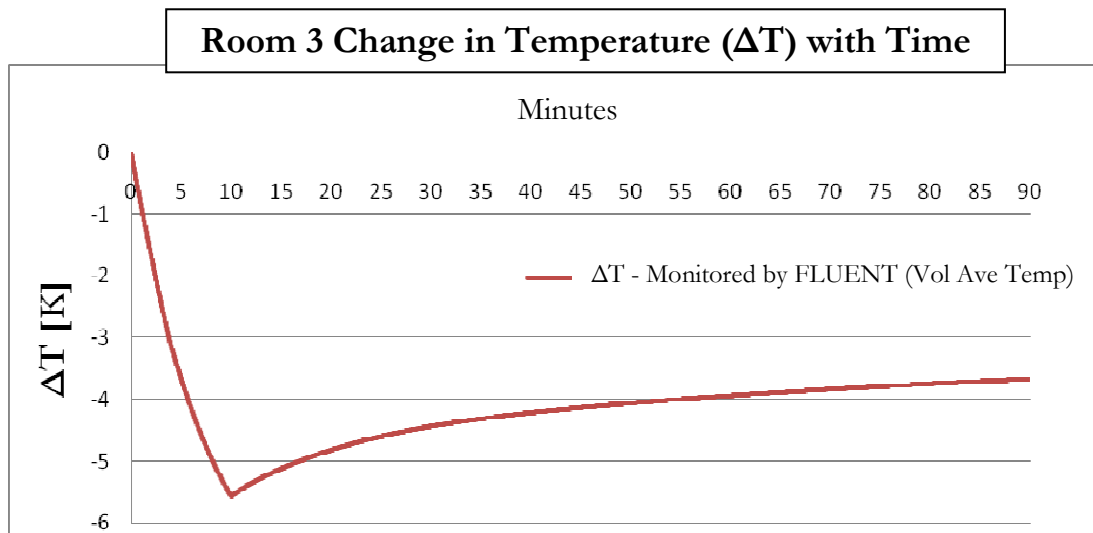**Figure 5.80 Room 3 change in temperature with time**

5.7 Comparison of Results for Three Ventilation Systems (Room 1, Room 2, and Room 3)

Comparing the change in the average volume temperature for the three rooms (Figure 5.81 & 5.82), it is clear that Rooms 2 and 3 reach much colder temperatures over Room 1 in ten minutes. Note that the total inlet vent areas and mass flow rates are the same for all the three rooms (the same amount of cold air was pumped into each room). The temperature change is the best indicator of thermal comfort. From the graph of the temperature change of Room 2 and Room 3 with respect to Room 1 (Figures 5.82), after the ten minutes, we note that Room 2 achieves a 5.9 K drop in temperature, which, when compared to the temperature drop for Room 1, is a 1.1 K (2.0^0 F) difference in room temperatures (Figure 5.83). This temperature difference yields a 22.1% decrease in temperature of Room 2 compared to Room 1(Figure 5.84). As mentioned earlier, there is typically a 30 – 60% reduction in energy required for cooling with the displaced ventilation system compared to overhead standard VAV ventilation system; our results are in the same ballpark. In literature it has been shown that there is a 30% reduction in volumetric airflow for achieving the same level of thermal comfort with displacement ventilation system compared to that needed for standard VAV system [Flonomix, 2009], this calculation is not performed in this thesis.

Analyzing the results for Room 3 (Figure 5.84) at the end of the ninety minute cycle, it can be concluded that Room 3 has achieved a 600% decrease in temperature over Room 1.

Room 3 has the chilled ceiling which provides radiative cooling for the entire 90 minutes of the simulation and it adds to the energy required for cooling Room 3. As mentioned earlier, a cooling tower (running on solar energy) alone can supply much of the necessary cooling load in many parts of the world. However, in case a cooling tower cannot cool the water of a hydronic system to the required temperature, it can at least pre-cool the water for a mechanical system to reduce the cooling load. In addition, by reducing the space necessary for large ventilation ducts in standard VAV systems and requiring significantly smaller mechanical heating/cooling units by reducing the heating/cooling loads, and a whole host of other changes [Harvey, 2009], the displacement ventilation with radiant cooling offers a superior system in most geographical regions, including the US, Europe, and Canada. Furthermore, in addition to using less primary energy and increasing the thermal comfort, such systems cost less to build in the commercial sector [Ürge-Vorsatz, Harvey, Mirasgedis, & Levine, 2007].
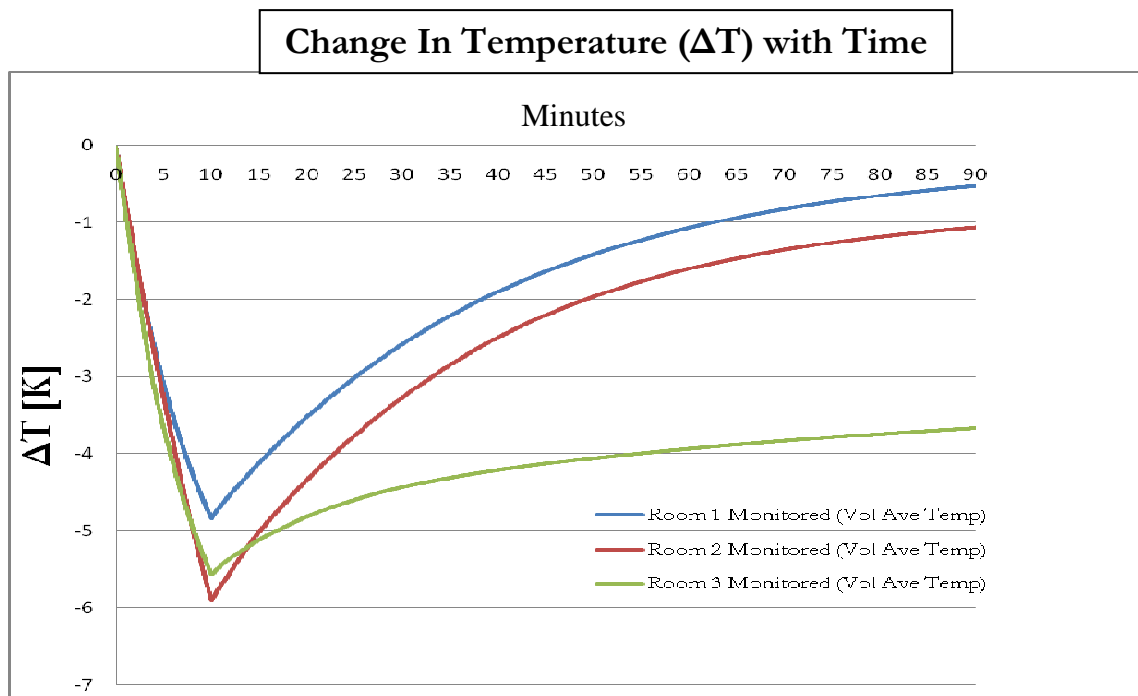
Figure 5.81 Change in volume-average temperature with time for Rooms 1, 2, and 3
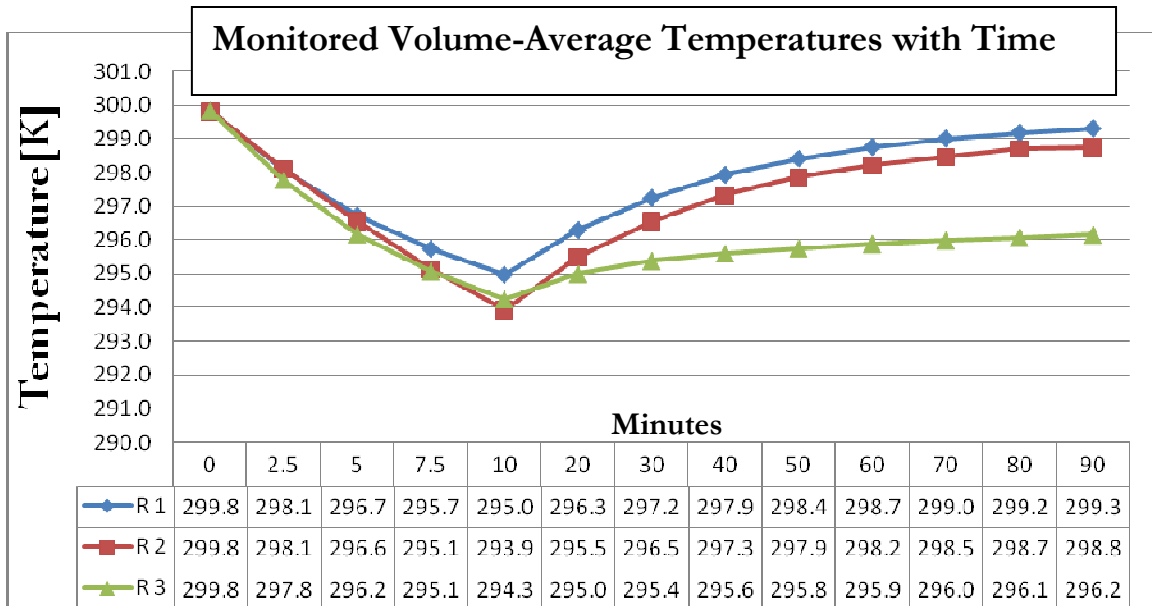
Figure 5.82 Monitored volume-average temperatures with time for Rooms 1, 2, and 3
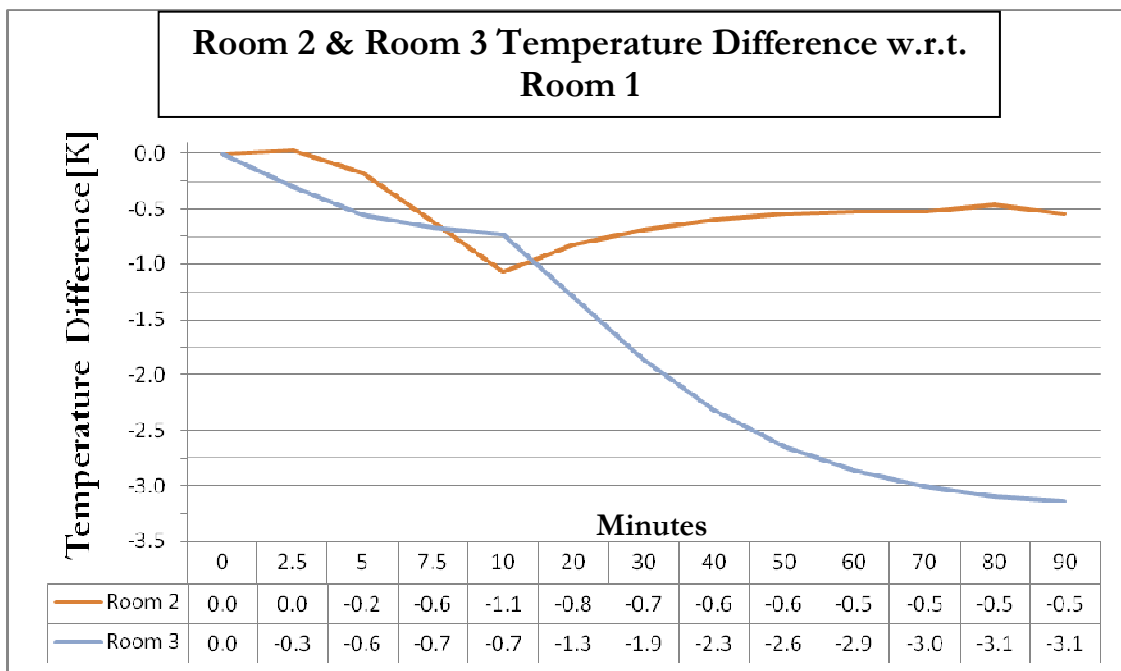
Figure 5.83 Rooms 2 & 3 temperature difference with time w.r.t. Room 1
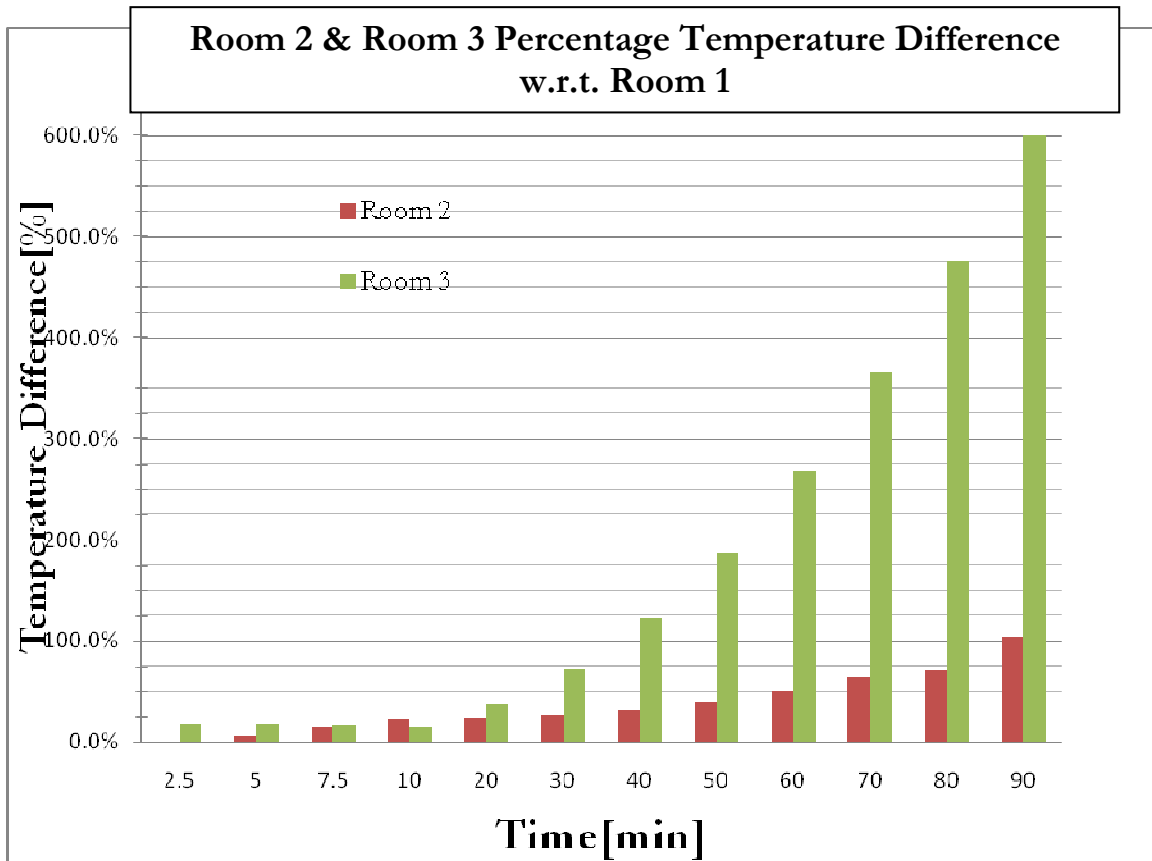
Figure 5.84 Rooms 2 & 3 percentage temperature difference with time w.r.t. Room 1

5.8   Conclusions

For the three different ventilation systems considered in this chapter, we have attempted to show the difference in the energy requirements and the thermal comfort levels for the three different cooling systems using CFD. From the calculations, it can be concluded that the displacement ventilation with chilled ceiling provides the most efficient cooling system along with the highest level of thermal comfort. However, experimental data is needed for validation of CFD results.

Chapter 6

Conclusions

In Chapter 4, we attempted to show that the 2-D flow field of natural convection in a rectangular box can be accurately calculated using CFD. The computations compared reasonably well with the experiment of Olsen, Glicksman, and Ferm (1990) for flow patterns inside the box capturing the turbulent, laminar, and secondary flow regions inside the box. Minor differences were found between the computation and the experiment for the temperature profiles; it is likely that these small differences in the thermal stratification were due to the different fluids used in the experiment (R114 gas) and the computation (air), since the air would have slightly more thermal stratification than the R114 gas.

Some of these differences could also be attributed to the fact that the computation was strictly 2-D while the experiment was performed in a 3-D enclosure. Nevertheless, there was reasonable agreement between the computation and the experiment. These calculations were performed for validation of CFD methodology.

In chapter 5, using Computational Fluid Dynamics (CFD), three different cooling systems used in contemporary office environments were modeled to compare energy consumption and thermal comfort levels. Incorporating convection and radiation technologies, full-scale models of an office room were employed to compare three ventilation systems: (a) an all-air overhead system (Variable-Air-Volume ventilation), (b) an all-air raised floor system (displacement ventilation), and (c) a combined air and hydronic radiant system (displacement ventilation with a chilled ceiling). The computational domain for each model consisted of one isothermal wall (simulating an exterior wall of the room) and adiabatic conditions for the remaining walls, floor, and ceiling (simulating interior walls of the room).

For the three different ventilation systems considered, we attempted to show the difference in the energy requirements and the thermal comfort levels for the three different cooling

systems. From the calculations, it was concluded that the displacement ventilation with chilled ceiling provided the most efficient cooling system along with the highest level of thermal comfort. However, experimental data is needed for validation of CFD results.

Chapter 7

Future Work

1. Experiments should be performed to validate the 3-D CFD results of Chapter 5.

2. Once the CFD results are validated, it should be straight forward to modify the room geometry to incorporate doors, windows, furniture, occupants, office equipment, exterior radiation, and any other features that can influence the cooling effects in the room. FLUENT has a solar ray tracing algorithm, which allows the user to specify geographical coordinates and then the program automatically predicts the direct illumination energy associated with the sun. Thus, once the overall cooling strategy is decided, it is quite simple to make a few modifications and numerically simulate a particular ventilation system in various geographical regions. CFD simulations can provide a direct comparison of energy and cost savings for a particular ventilation system for cooling in different climates. CFD can also be used to optimize the performance envelope of residential and commercial buildings.

3. The thermal properties of building materials should also be included in the simulations. As an example one can include a layer of phase change material (PCM) in the construction of walls and window curtains etc, which can improve the performance envelope of the room/building.

Appendix A:

Air density table

Piecewise-Linear Profile of Variation of Air Density with Temperature [WAsP, 2009]	
Temperature (K)	Density (kg/m3)
273.15	1.293
288.16	1.225
293.15	1.205
298.15	1.184
303.15	1.164
308.15	1.145
313.15	1.127

References

"Air Density Table." *WAsP*. Web. Aug.2009.
<http://www.wasp.dk/support/FAQ/WebHelp/AirDensityTable.htm>.

Ansys Inc. FLUENT. Computer software. Ver. 6.3, 2007

Ansys Inc. GAMBIT. Computer software. Ver. 6.2, 2007

ASHRAE. Fundamentals ASHRAE handbook. Atlanta, GA: American Society of Heating,
Refrigeration and Air Conditioning Engineers, 1977

Balaji, C., M. Hölling, and H. Herwig. "Nusselt number correlations for turbulent natural
convection flows using asymptotic analysis of the near-wall region." *Journal of Heat
Transfer* 129 (2007): 1100-104.

"Building Sector, Energy, CO2 Emissions - Current Situation - Architecture 2030." *Climate
Change, Global Warming, and the Built Environment - Architecture 2030*. Web. 1 Aug. 2009.
<http://www.architecture2030.org/current_situation/building_sector.html>.

Carnegie Endowment for International Peace. Web. Aug. 2009.
<http://www.globalization101.org/index.php?file=issue&pass1=subs&id=326]>.

Çengel, Yanus A., Robert H. Turner, *Fundamentals of Thermal-Fluid Sciences*, New York, NY:
McGraw-Hill, 2001

Chen, Q. "Comparison of different k-ε models for indoor air flow computations." *Numer.
Heat Transfer* (1995) B23: 269-88.

Chen, Z. D., Y. Li, and J. Mahoney. "Natural ventilation in an enclosure induced by a heat
source distributed uniformly over a vertical wall." *Building and Environment* 36 (2001):
493-501.

European Commission (2001) *Directive of the European Parliament and the Council on the Energy
Performance of Buildings; Explanatory Memorandum*
(http://www.climnet.org/EUenergy/ENbuildings.pdf).

Farhangnia, M., S. Biringen, and L. J. Peltier. "Numerical simulation of two-dimensional
buoyancy-driven turbulence in a tall rectangular cavity." *International Journal For
Numerical Methods In Fluids* 23 (1996): 1311-326.

Fitzgerald, Shaun D., and Andrew W. Woods. "Natural ventilation of a room with vents at
multiple levels." *Building and Environment* 39 (2004): 505-21.

Flonomix. "Thermal Displacement Ventilation." *Splash*. Web. 14 Aug. 2009.
<http://www.flonomix.com/thermal_displacement_ventilation.htm>.

George, W. K. and S. P. Cap, "A theory for natural convection turbulent boundary layer next to heated vertical surfaces" *International J. Heat & Mass Transfer* (1979) 22 pp. 813-826

Glicksman, Leon R. "Energy efficiency in the built environment." *Physics Today* 61.7 (2008): 35.

Harvey, L. D. "Reducing energy use in buildings sector: measures, costs, and examples." *Energy Efficiency* 2 (2009): 139-63.

He, G., X. Yang, and J. Srebric. "Removal of contaminants released from room surfaces by displacement and mixing ventilation: modeling and validation." *Indoor Air* 15 (2005): 367-80.

Henkes, R. A. W. M. Natural-Convection Boundary Layers. Ph. D Thesis. Deltf University of Technology Delft, The Netherlands (1990).

Henkes, R. A. W. M. and C. J. Hoogendoorn, Comparison of turbulence models for the natural convection boundary layer along a heated vertical plate. *International J. Heat & Mass Transfer.* (1989) 32(1), 157-169.

Henkes, R. A. W. M. and C. J. Hoogendoorn, Comparison exercise for computations of turbulent natural convection in enclosures. *Numerical Heat Transfer,* (1995) Part B. 28, 59-78.

Hölling C., M. and H. Herwig, "Asymptotic analysis of heat transfer in turbulent Rayleigh Benard convection." *International J. Heat & Mass Transfer.* (2006) to be published

Howell, S. A., and I. Potts. "A comparison of predictive techniques for natural displacement ventilation of buildings." *Proc. CIBSE Nat. Conf.* (1998): 156-64.

Howell, Ronald H, Harry J. Saur, William J. Coad, *Principles Of Heating Ventilation and Air Conditioning*, New York, NY: American Society of Heating, Refrigerating and Air-Conditioning, 1998

Howell, S. A., and I. Potts. "On the natural displacement flow through a full-scale enclosure, and the importance of the radiative participation of the water vapour content of the ambient air." *Building and Environment* 37 (2002): 817-23.

Ince, N. Z. & B. E. Launder, 1989 On the computation of buoyancy-driven turbulent flows in rectangular enclosures. *Intl. J. Heat & Fluid Flow.* 10(2), 110-117

Koomey, J.G., Webber, C.A., Atkinson, C.S., Nicholls, A. and Holloman, B. (2000) Buildings sector, in *Scenarios for a Clean Energy Future.* ORNL/CON-476, Oak Ridge National Laboratory, Oak Ridge, TN.

Linden, P. F. "The fluid mechanics of natural ventilation." *Annu. Rev. Fluid Mech.* 31 (1999): 291-38.

Livermore, S. R., and A. W. Woods. "On the effect of distributed cooling in natural ventilation." *J. Fluid Mech.* 600 (2008): 1-17.

Madireddi, Sesha. "Meshing Techniques." Personal interview. Mar. 2009.

NRCan (Natural Resources Canada) (2005) Energy Use Data Handbook, 1990 and 1997-2003, Office of Energy Efficiency, NRCan, Ottawa (http://www.oee.nrcan.gc.ca).

Olson, D. A., L. R. Glicksman, and H. M. Ferm. "Steady-state natural convection in empty and partitioned enclosures at high rayleigh numbers." *Journal of Heat Transfer* 112 (1990): 640-47.

Tieszen, S., A. Ooi, P. Durbin, and M. Behnia. "Modeling of natural convection heat transfer." *Proceedings of the Centre for Turbulence Research, Stanford University, CA* (1998): 287-301.

Ürge-Vorsatz, Diana, L. D. Harvey, Sevastianos Mirasgedis, and Mark D. Levine. "Mitigating CO_2 emissions from energy use in the world's buildings." *Building Research and Information* 35.4 (2007): 379-98.

US Department of Energy. Energy Information Administration. *Table E1A. Major Fuel Consumption (Btu) by End Use for All Buildings, 2003. Http://www.eia.doe.gov/emeu/cbecs/cbecs2003/detailed_tables_2003/2003set19/2003pdf/e1a-e11a.pdf.* Sept. 2008. Web. Aug. 2009.

Wan, M. P., and C. Y. Chao. "Numerical and experimental study of velocity and temperature characteristics in a ventilated enclosure with underfloor ventilation systems." *Indoor Air* (2005).

Zhao, Bin, Ying Zhang, Xianting Li, Xudong Yang, and Dongtao Huang. "Comparison of indoor aerosol particle concentration and deposition in different ventilated rooms by numerical method." *Building and Environment* 39 (2004): 1-8.

Vita

Andrew K. Harris

Date of Birth February 27, 1982

Place of Birth Caldwell, Idaho

Degrees   College of Idaho
      B.S. Physics and Mathematics
      May 2004

      Washington University in St. Louis
      M.S., Mechanical Engineering
      August 2009

Energy Demand in Commercial Buildings   Andrew Harris, M.S. 2009